PALEOCEANOGRAPHY, VOL. 22, PA1209, doi:10.1029/2006PA001285, 2007

A paleomagnetic approach toward refining Holocene radiocarbon-based chronologies: Paleoceanographic records from the north Iceland (MD99-2269) and east Greenland (MD99-2322) margins

Joseph S. Stoner,[1] Anne Jennings,[2] Gréta B. Kristjánsdóttir,[2] Gita Dunhill,[2] John T. Andrews,[2] and Jorunn Hardardóttir[3]

Received 16 February 2006; revised 31 August 2006; accepted 11 October 2006; published 23 February 2007.

[1] We report the intercalibration of paleomagnetic secular variation (PSV) and radiocarbon dates of two expanded postglacial sediment cores from geographically proximal, but oceanographically and sedimentologically contrasting settings. The objective is to improve relative correlation and chronology over what can be achieved with either method alone. Core MD99-2269 was taken from the Húnaflóaáll Trough on the north Iceland shelf. Core MD99-2322 was collected from the Kangerlussuaq Trough on the east Greenland margin. Both cores are well dated, with 27 and 20 accelerator mass spectrometry ^{14}C dates for cores 2269 and 2322, respectively. Paleomagnetic measurements made on u channel samples document a strong, stable, single-component magnetization. The temporal similarities of paleomagnetic inclination and declination records are shown using each core's independent calibrated radiocarbon age model. Comparison of the PSV records reveals that the relative correlation between the two cores could be further improved. Starting in the depth domain, tie points initially based on calibrated ^{14}C dates are either adjusted or added to maximize PSV correlations. Radiocarbon dates from both cores are then combined on a common depth scale resulting from the PSV correlation. Support for the correlation comes from the consistent interweaving of dates, correct alignment of the Saksunarvatn tephra, and the improved correlation of paleoceanographic proxy data (percent carbonate). These results demonstrate that PSV correlation used in conjunction with ^{14}C dates can improve relative correlation and also regional chronologies by allowing dates from various stratigraphic sequences to be combined into a single, higher dating density, age-to-depth model.

Citation: Stoner, J. S., A. Jennings, G. B. Kristjánsdóttir, G. Dunhill, J. T. Andrews, and J. Hardardóttir (2007), A paleomagnetic approach toward refining Holocene radiocarbon-based chronologies: Paleoceanographic records from the north Iceland (MD99-2269) and east Greenland (MD99-2322) margins, *Paleoceanography*, *22*, PA1209, doi:10.1029/2006PA001285.

1. Introduction

[2] Paleoclimatology has recently focused on high-temporal-resolution records [e.g., *Hodell et al.*, 2001; *Wang et al.*, 2005; *Ellison et al.*, 2006] in an effort to derive societally relevant information on past conditions. Continental margin settings, where sediments can accumulate at rates of meters per thousand years, hold significant promise for defining environmental change at centennial or even higher resolutions potentially through the Holocene and beyond. Yet, it is rarely possible to develop chronologies accurate enough to fully exploit these resolution gains. Radiocarbon dating, which remains the primary tool for constructing reliable Holocene and late glacial chronologies, is restricted by the availability of suitable material for dating. Even when radiocarbon dates are easily obtained, $1-\sigma$ uncertainties in measurement precision propagate during calibration to calendar age probability ranges from ~50 years to more than several centuries through the Holocene [*Stuiver et al.*, 1998; *Reimer et al.*, 2004; *Guilderson et al.*, 2005]. Additional sources of radiocarbon dating uncertainties result from incomplete knowledge of the magnitude and variability of the marine radiocarbon reservoir age, as well as a myriad of other natural and sediment retrieval factors. Even if the dates are accurate, construction of an age model results in additional uncertainties [*McMillan et al.*, 2002; *Telford et al.*, 2004]. These uncertainties are only compounded when comparing two or more sites. Therefore new chronological and stratigraphic techniques and strategies must be developed if we are to fully realize the promise provided by rapidly deposited sediments.

[3] The Earth's magnetic field has undergone significant directional (declination and inclination) changes during the Holocene [e.g., *Thompson*, 1984; *Korte et al.*, 2005]. Geomagnetic directional changes, known as paleomagnetic secular variation (PSV), have been used as a dating method for more than 30 years [e.g., *Thompson*, 1973]. Recent studies have brought renewed attention to the Holocene PSV record [e.g., *Lund*, 1996; *Stockhausen*, 1998; *Snowball and Sandgren*, 2002; *St-Onge et al.*, 2003; *Ojala and*

[1]College of Oceanic and Atmospheric Sciences, Oregon State University, Corvallis, Oregon, USA.

[2]Institute of Arctic and Alpine Research, University of Colorado, Boulder, Colorado, USA.

[3]National Energy Authority, Reykjavik, Iceland.

0883-8305/07/2006PA001285$09.00

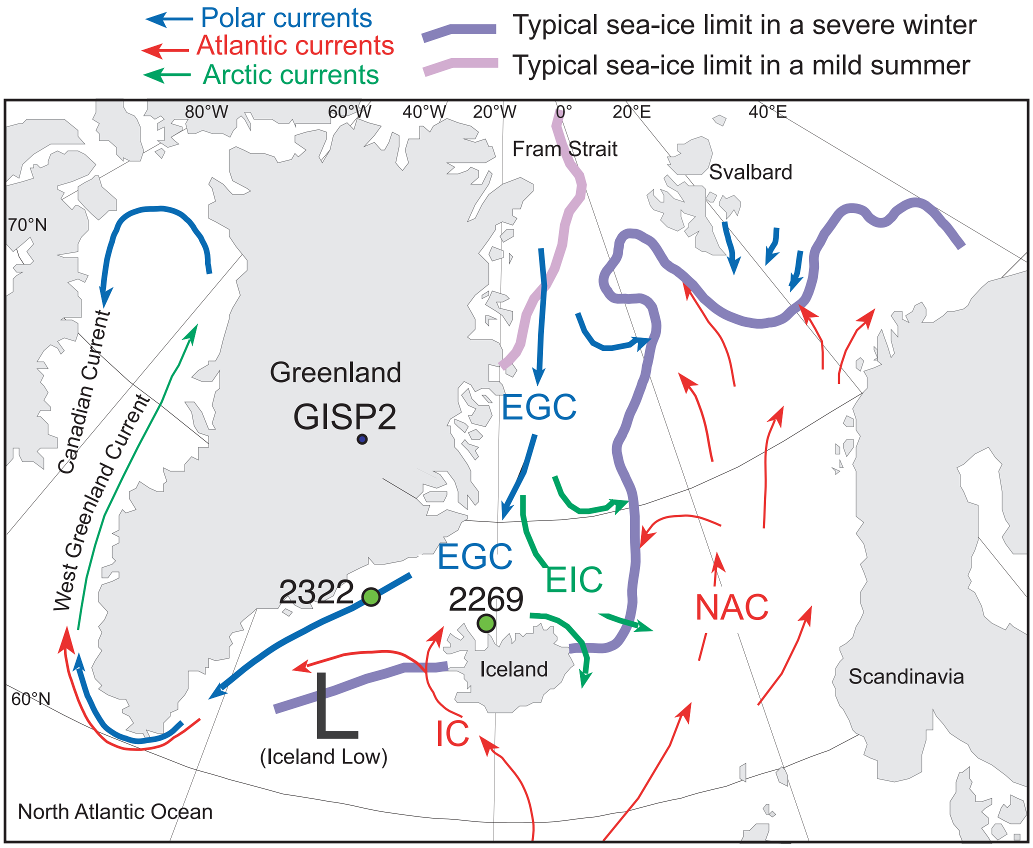

Figure 1. Location map of core sites studied. Cores MD99-2322 and MD99-2269 were taken from shelf basins where sediment sequences accumulated in thick stratified sections unaffected by iceberg scouring. Core MD99-2269 (latitude 66°37.53 N, longitude 20°51.16 W, water depth 365 m, length 2533 cm) is from Húnaflói, on the north Iceland shelf. Core MD99-2322 (latitude 67°08.18 N, longitude 30°49.67 W, water depth 714 m, length 2617 cm) is from the deepest part of the Kangerlussuaq trough, SE Greenland shelf. Abbreviations are as follows: EGC, East Greenland Current; EIC, East Iceland Current; NAC, North Atlantic Current; IC, Irminger Current; NAC, North Atlantic Current; and GISP2, Greenland Ice Sheet Project 2. Modified from *Jennings et al.* [2006], reprinted with permission from Elsevier.

Saarinen, 2002; *Irurzun et al.*, 2006; *Vigliotti*, 2006] and its use as a dating method [*Saarinen*, 1999; *Kotilainen et al.*, 2000; *Breckenridge et al.*, 2004; *St-Onge et al.*, 2004]. Comparisons in restricted regions (Finland) demonstrate that age uncertainties associated with correlating distinct PSV features are no greater than varve count uncertainty (∼±1%) for the last 6000 years [*Ojala and Tiljander*, 2003]. Comparison and intercalibration of PSV and radiocarbon dates in the marine realm has up to now received little attention.

[4] Here we use PSV correlations in conjunction with a high density of radiocarbon dates from two high-accumulation-rate sediment cores recovered using the R/V *Marion Dufresne II* Calypso corer from the north Iceland (MD99-2269) and east Greenland (MD99-2322) continental margins (Figure 1) to (1) begin documenting the Holocene PSV record of the region, (2) improve the relative correlation between the two records, and (3) reduce chronological uncertainty and improve the calibrated radiocarbon chronology for each core. The immediate relevance of the presented PSV correlation is demonstrated because paleoceanographic proxies from the north Iceland (MD99-2269) and east Greenland (MD99-2322) continental margins show broad similarities on millennial timescales (Figure 2) suggesting a common response to ocean circulation changes. Whether this similarity extends to the centennial regime is difficult to ascertain using radiocarbon chronologies alone. Given the oceanographic settings of the two cores, one could argue for either synchronous or nonsynchronous processes at centennial timescales. Therefore understanding paleoceanographic dynamics of this region is critically linked to chronological uncertainties.

2. Region of Study

[5] The cores studied were collected during the summer of 1999 as part of the international IMAGES-V (International Marine Past Global Change Study) campaign aboard the *Marion Dufresne II*. These sites were targeted because of the expanded postglacial sediment sections preserved in shelf basins where sediments have accumulated in thick stratified sections unaffected by iceberg scouring. Core

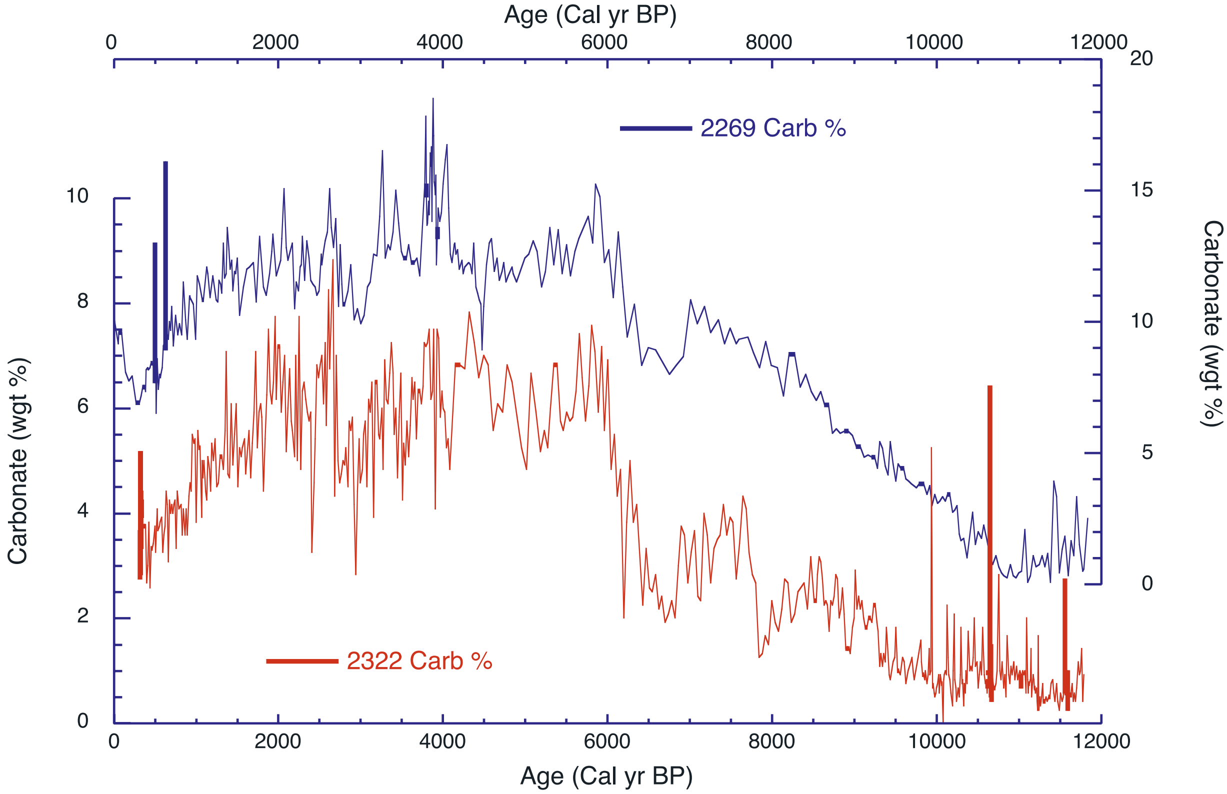

Figure 2. Comparison of weight percent carbonate ($CaCO_3$) records from cores MD99-2322 (red) and MD99-2269 (blue) on their independent calibrated radiocarbon chronologies based on the linear interpolated age model (Figure 3). The $CaCO_3$ record is interpreted as a proxy for productivity throughout the water column. It reflects both the contribution of Atlantic Water in the Irminger Current over the core sites balanced by outflow of Arctic and polar surface waters. Much of the carbonate is from coccolith production, augmented by foraminiferal production [*Giraudeau et al.*, 2004].

MD99-2322 (latitude 67°08.18 N, longitude 30°49.67 W, water depth 714 m, length 2617 cm) (hereinafter referred to as core 2322) is from the deepest part of the Kangerlussuaq Trough, SE Greenland shelf (Figure 1). Core MD99-2269 (latitude 66°37.53 N, longitude 20°51.16 W, water depth 365 m, length 2533 cm) (hereinafter referred to as core 2269) was raised from Húnaflói, on the north Iceland shelf (Figure 1). The sediments of both cores are homogenous silty clays that are olive gray for core 2269 and dark gray for core 2322. Core 2322 also contains occasional millimeter to centimeter thick sandy silt lenses and dispersed >1 mm grains. Rhyolitic tephra shards were found in the core catchers of both cores. Rhyolitic shards from the core catcher of core 2269 and from the basal sample of core 2322 (2613–2614 cm) were geochemically confirmed to be Vedde Ash, a well-known chronostratigraphic marker in the region (10,300 ^{14}C years B.P. [*Bard et al.*, 1994], 11,980 ± 80 calendar (cal) years B.P. [*Grönvold et al.*, 1995]). Brown basaltic tephra encountered in both cores has proved to be the early Holocene tephra marker, the Saksunarvatn tephra (8.9–9.0 ^{14}C kyr B.P. [*Mangerud et al.*, 1986] 10,180 cal years B.P. ±60 [*Grönvold et al.*, 1995]). The Saksunarvatn tephra occurs as a visible layer in core 2269 [*Andrews et al.*, 2002], whereas in core 2322 it was located by grain counts and identified by geochemistry (K. Grönvold, Nordic Volcanological Institute).

[6] Oceanographically, the cores are from hydrographically stratified sites where fresher and colder northern source waters overlie warmer and saltier Atlantic source waters. Core 2322 is situated where Irminger Intermediate Water (IIW) flows into the trough from the southeast between the cold, low-salinity Polar Water of the East Greenland Current (EGC), above and Atlantic Intermediate water (AIW) from return Atlantic Water of the Norwegian Atlantic Current, below [*Aagaard and Coachman*, 1968a, 1968b; *Jennings et al.*, 2002, 2006]. The extent of the inflow of warm water varies substantially from year to year. While core 2269 is located in the warmer of the two sites with north Iceland strongly influenced by Atlantic Water in the North Iceland Irminger Current (NIIC), it is also affected by colder and fresher Polar and Arctic Water carried in the East Iceland Current (EIC) [*Stefansson*, 1962; *Hopkins*, 1991; *Giraudeau et al.*, 2004]. The two sites are similarly influenced by IIW. Surface water conditions, however, differ, with the east Greenland location constantly influenced by Polar Water flow of the EGC while the Iceland site has more variable surface water conditions with intermittent incursions of Polar Water onto the north Iceland shelf. Paleoceanographically, it is therefore possible that these

Table 1. Accelerator Mass Spectrometer Radiocarbon Measurements and Calibrated (Calendar) Ages for Cores MD99-2269 and MD99-2322[a]

Core	Depth Central, cm	INSTAAR Laboratory Number	Radiocarbon Laboratory Number	Material Dated	Weight, mg	Reported Age, ^{14}C years B.P.	Median Probability, cal years B.P.	Minimum 1 σ, cal years B.P.	Maximum 1 σ, cal years B.P.
MD99-2322	2.5	1612-S	C5734	*Astarte* sp.	83.2	675 ± 30	322	277	360
MD99-2322	34	1592-S	AA40050	*Colus turgidulus*	16.7	693 ± 38	344	290	385
MD99-2322	101.5	1658-S	AA49380	mixed forams	5	1267 ± 44	812	761	875
MD99-2322	150	1659-S	AA49381	bivalve	18.3	1627 ± 46	1191	1146	1250
MD99-2322	368	1660-S	AA49382	bivalve	17.5	3451 ± 39	3332	3280	3381
MD99-2322	564	1593-S	AA40051	scaphopod	6.9	4899 ± 55	5213	5125	5299
MD99-2322	771	1594-S	AA40052	shell fragments	2	6115 ± 65	6545	6467	6626
MD99-2322	1073	1595-S	AA40053	*Nuculana buccata*	6.4	8000 ± 300	8522	8170	8883
MD99-2322	1298	1596-S	AA40044	*Nuculana pernula*	28.2	8609 ± 67	9272	9189	9385
MD99-2322	1393	1635-S	AA43351	*Nuculana pernula*	35.2	8877 ± 62	9535	9466	9595
MD99-2322	1432	1636-S	AA43352	*Bathyarca glacialis*	98.9	8999 ± 61	9679	9552	9755
MD99-2322	1516	1637-S	AA43353	*Nuculana buccata*	10	9108 ± 65	9859	9716	9999
MD99-2322	1807	1638-S	AA43354	*Nuculana buccata*	14.4	9514 ± 81	10369	10273	10466
MD99-2322	1908	1639-S	AA43355	*Nuculana buccata*	20.4	9747 ± 76	10616	10519	10692
MD99-2322	2006	1640-S	AA43356	*Nuculana buccata*	27	9803 ± 64	10675	10567	10751
MD99-2322	2140	1641-S	AA43357	*Nuculana buccata*	14.1	10,034 ± 69	11017	10921	11143
MD99-2322	2342	1642-S	AA43358	*Nuculana buccata*	14	10,293 ± 77	11296	11180	11375
MD99-2322	2436	1643-S	AA43359	*Nuculana pernula*	18.8	10,442 ± 82	11547	11345	11706
MD99-2322	2542	1746-S	AA61216	benthic forams	3.4	10,480 ± 110	11621	11365	11851
MD99-2322[b]	2636	1564-S	AA36608	benthic forams	6.1	11,125 ± 80	12765	12707	12835
MD99-2269	1.0[c]	1583-S	AA38584	*Bathyarca glacialis*	172.2	72 ± 37			
MD99-2269	42.5[c]	1610-S	CURL-5732	*Arca glacialis*	185.7	680 ± 30	328	281	364
MD99-2269	131.0[c]	1611-S	CURL-5733	*Macoma* sp	13.5	1010 ± 30	590	556	623
MD99-2269	161.0[c]	1677-S	AA54589	cf. *Macoma balthica*	7.9	1124 ± 41	679	644	711
MD99-2269	177.5[c]	1584-S	AA38585	*Bathyarca glacialis*	88.1	1226 ± 25	762	718	795
MD99-2269	246.0[c]	1678-S	AA54593	mixed benthic forams	2.3	1535 ± 47	1091	1036	1161
MD99-2269	266.0[c]	1655-S	AA47785	*Macoma* sp.	8.6	1693 ± 42	1250	1210	1293
MD99-2269	351.0[c]	1703-S	AA57895	cf. *Yoldia glacialis*	67.3	1978 ± 35	1536	1489	1593
MD99-2269	412.0[c]	1679-S	AA54590	cf. *Macoma balthica*	6.9	2396 ± 47	2028	1966	2098
MD99-2269	456.0[c]	1585-S	AA38586	*Yoldia* cf. *myalis*	12.5	2578 ± 48	2247	2189	2315
MD99-2269	563.0[c]	1704-S	AA57896	*Yoldia* sp	19.1	3017 ± 39	2787	2741	2824
MD99-2269	621.0[c]	1680-S	AA54592	Mixed benthic forams	2.2	3375 ± 80	3237	3142	3345
MD99-2269	707.5[c]	1705-S	AA57897b	*Arca glacialis*	79	3840 ± 33	3793	3730	3845
MD99-2269	815.0[c]	1706-S	AA57898	*Yoldia* sp	2303	3949 ± 39	3939	3866	3992
MD99-2269	937.5[c]	1681-S	AA54591	cf. *Nucula*	25.4	4340 ± 46	4474	4407	4527
MD99-2269	974.0[c]	1542-S	AA35175	Unid. gastropod	14.5	4505 ± 50	4703	4638	4793
MD99-2269	1162.0[c]	1656-S	AA47786	*Yoldia* cf. *lenticula*	22	5296 ± 53	5657	5592	5704
MD99-2269	1268.0[c]	1707-S	AA57899	*Yoldia* sp.	4.1	5826 ± 51	6245	6192	6289
MD99-2269	1398.0[c]	1747-S	AA61217	mixed benthic forams	3.9	6833 ± 81	7351	7274	7419
MD99-2269	1519.5[c]	1586-S	AA38587	*Yoldia* cf. *glacialis*	9.5	7749 ± 62	8222	8159	8298
MD99-2269	1568.0[c]	1673-S	AA51435	*Macoma balthica*	5.5	8084 ± 57	8545	8458	8608
MD99-2269	1708.0[c]	1750-S	AA61220	*N. labradorica*	2.5	8572 ± 78	9219	9106	9330
MD99-2269[b]	1708.0[c]	1751-S	AA61221	*G. auriculata*	4.4	8609 ± 92	9263	9150	9392
MD99-2269	1718.0[c]	1708-S	AA57900a	Unid. molluscs	6.4	8590 ± 43	9251	9162	9325
MD99-2269	1980.5[c]	1543-S	AA35176	Unid. mollusc	10	9265 ± 70	10085	9966	10193
MD99-2269	2068.0[c]	1682-S	AA54594	mixed benthic forams	5.5	9477 ± 88	10336	10227	10425
MD99-2269[b]	2499.0[c]	1561-S	AA35805	mixed benthic forams	6.2	10920 ± 85	12489	12351	12672

[a]Calibrated using Calib 5.0 [*Stuiver and Reimer*, 1993] and the updated marine calibration data sets [*Hughen et al.*, 2004].
[b]Not used in age model.
[c]Gap-corrected depths.

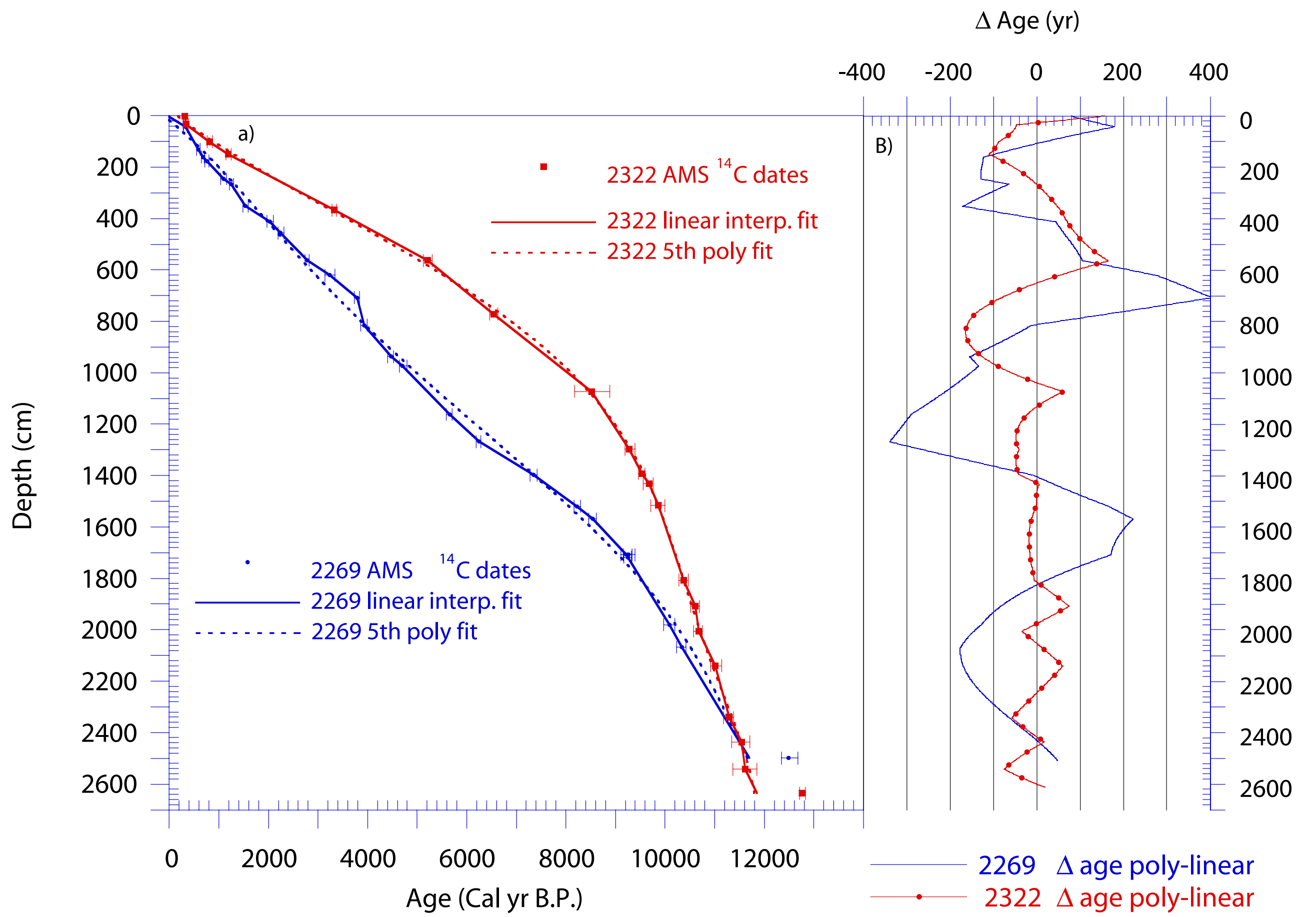

Figure 3. (a) The age-depth profiles of calibrated (Calib 5.0) [*Stuiver and Reimer*, 1993] radiocarbon dates using a standard marine reservoir correction [*Hughen et al.*, 2004] from piston cores MD99-2322 (red) and MD99-2269 (blue) (Table 1). The basal ages of the cores were constrained by assuming constant sedimentation rates defined by the overlying calibrated radiocarbon dates (as described in the text). Basal age estimates are 11,700 calendar (cal) years B.P. for core 2269 and 11,850 cal years B.P. for core 2322. Linear interpolation and fifth-order (the highest-order polynomial that could be stably fit to the data) polynomial fits are shown. Error bars on dates equal maximum $1-\sigma$ spread of all calibrated age ranges. (b) Age difference between the linear interpolation and polynomial fit for cores MD99-2322 (red) and MD99-2269 (blue).

sites could have contrasting or similar circulation histories at different timescales.

3. Materials and Methods

3.1. Paleomagnetic Methods

[7] The low-field volumetric magnetic susceptibility and gamma ray attenuation (GRA) bulk density were measured shipboard at 2-cm intervals using a GEOTEK™ MST (Multi Sensor Track). The cores were split and described on board the *Marion Dufresne II*. Color was determined by spectrophotometry on the newly split face of the core at 5-cm intervals. U channels were taken (rigid u-shaped plastic liners with a square 2-cm cross section and a length up to 1.5 m) from the split cores. Paleomagnetic measurements were made using progressive, alternating field (AF) demagnetization at the Paleomagnetism Laboratory at the University of California, Davis (UCD) using a 2-G Enterprises™ Model 755 cryogenic magnetometer. The u channel samples were measured at 1-cm intervals prior to and after applying peak fields of 10, 20, 30, 40, 50, and 60 mT for core 2269 and 10, 20, 25, 30, 35, 40, 50, and 60 mT for core 2322. The response function of the magnetometer's pickup coils is such that each measurement integrates across a ~4.5 cm stratigraphic interval [*Weeks et al.*, 1993]. To eliminate edge effects, data from the ends (top and bottom 4-cm) of each u channel are not used to eliminate edge effects. The upper 60 cm of core 2269 (~270 cal years B.P.) was not sampled because of soft sediment deformation. Other intervals possibly affected by soft sediment deformation are not considered.

3.2. Radiocarbon Methods

[8] The initial age models for cores 2269 and 2322 are based on 27 and 20 accelerator mass spectrometry (AMS) radiocarbon dates, respectively [*Dunhill et al.*, 2004]. Dates

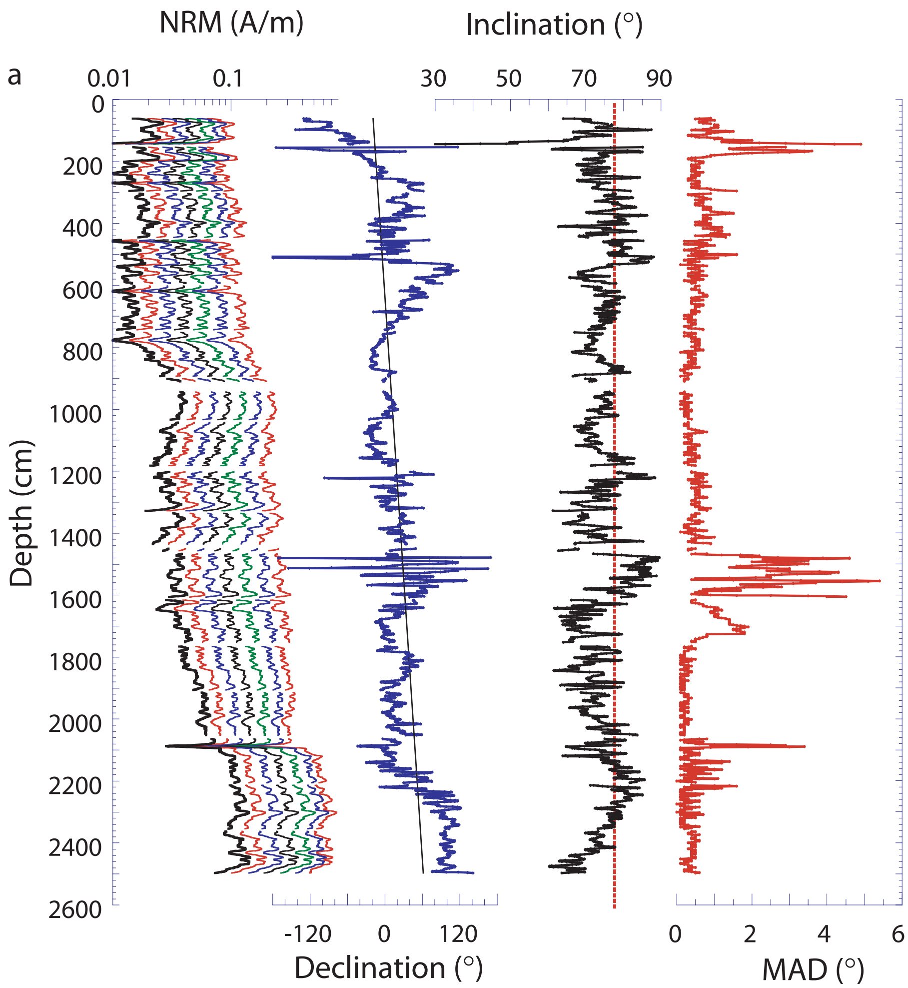

Figure 4. Down-core plot of natural remanent magnetization (NRM) intensity at all demagnetization steps, characteristic remanent magnetization (ChRM) declination and inclination, both calculated from the 10 to 60 mT steps using the method of *Kirschvink* [1980], and the maximum angular deviation (MAD) values of the ChRM fits for (a) cores MD99-2269 and (b) MD99-2322. The dashed vertical line on the inclination plots represents the expected inclination at the site location for a geocentric axial dipole. Solid line for the core 2269 declination represents the linear fit to the data, which suggests that rotation occurred during coring. MAD values under 10° are generally considered to reflect a well-defined magnetic vector.

were determined from mollusks, benthic and planktic foraminifera and gastropods (Table 1 and Figures 3a and 3b). The dates were calibrated to calendar years using CALIB 5.0 [*Stuiver and Reimer*, 1993] and the updated marine calibration data sets [*Hughen et al.*, 2004] with a standard marine reservoir correction (~400 years) applied to all dates from both cores. Prior to the development of the initial chronology for core 2269 three voids were "closed" to remove accumulation rate artifacts that would result from the increased core length. Voids occurred at 937–946 cm, 1204–1208 cm and 1457–1477 cm. Closure of voids resulted in a reduction in the total length of the core from 2533 to 2507 cm.

3.3. Paleoenvironmental Data Methods

[9] For carbonate analysis in core 2269, 2-cm-wide discrete sediment samples were taken at 5-cm intervals to a depth of 1000 cm and then every 10 cm thereafter. In core 2322, 1-cm-wide carbonate samples were taken every 2 cm until a depth of 450 cm and then every 6 cm thereafter. The samples were air dried and sieved through a 2-mm mesh screen. The <2 mm material was ground to a powder using a mortar and pestle. Carbonate content was measured using a Coulometer Model CM5012. The difference on replicate runs using this instrument is 0.04 ± 0.22% [*Andrews et al.*, 2001].

4. Results

4.1. Calibrated Radiocarbon Dates for Cores 2269 and 2322

4.1.1. Age to Depth Relationships

[10] Calibrated AMS ^{14}C dates to the age-depth relationships for cores 2269 and 2322 are shown in Figure 3 and

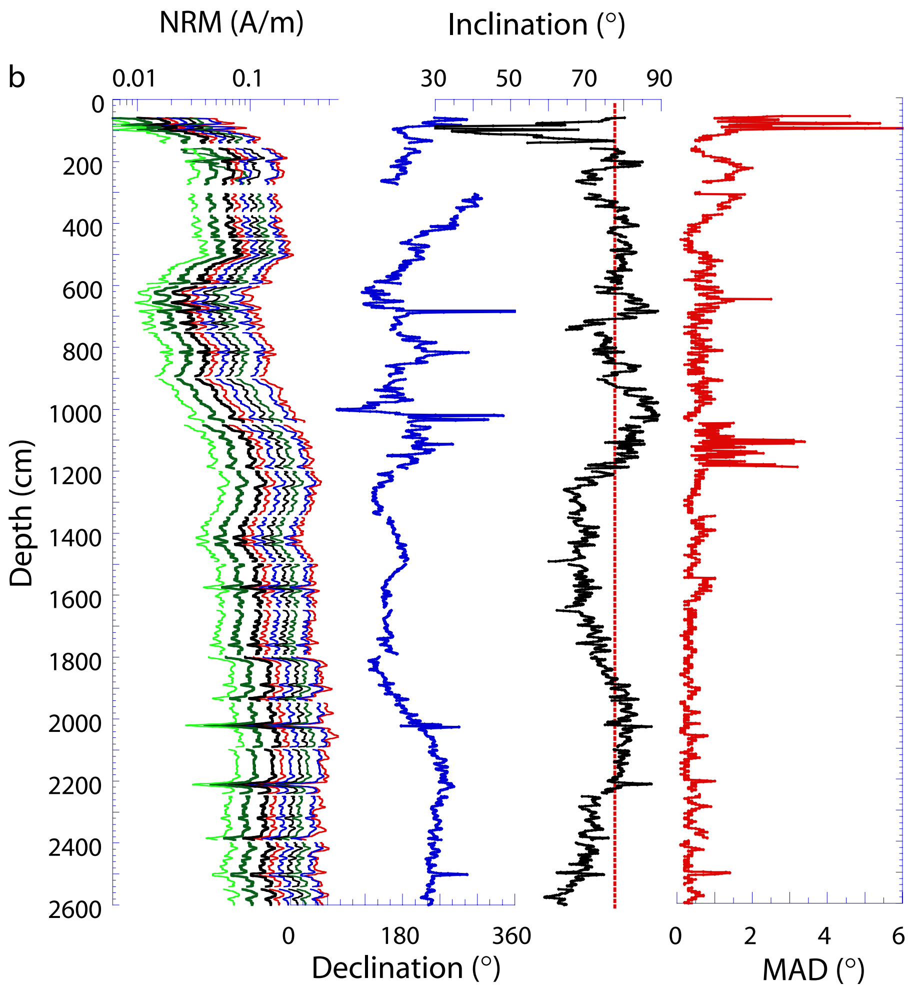

Figure 4. (continued)

Table 1. Radiocarbon dates in core 2269 are concentrated from 0–8500 cal years B.P. (ca 0–16 m) and occur at lower density from 8500 to 12500 cal years B.P. In core 2322 the highest density of dates occurs from approximately 9000 to 12000 cal years B.P. (ca 13–25.5 m), whereas the density of dates is lower from 1200 to 9000 cal years B.P. (ca 1.5–13 m). The distribution of dates reflects the occurrence of dateable material and patterns of sediment accumulation. Sedimentation rates are relatively uniform throughout 2269 core (~2 m/kyr). In contrast, core 2322 has 2 distinct modes, with a sedimentation rate around 1 m/kyr for the upper 9 kyr (~11 m) to more than 5 m/kyr below.

[11] An earlier age model for core 2269 [e.g., *Andrews et al.*, 2003] was derived from 11 calibrated radiocarbon dates and the Saksunarvatn tephra (10,180 ± 60 years [*Grönvold et al.*, 1995]). A linear regression with the expression: age (cal years B.P.) = 322.8 ± 92 + 4.9 ± 0.07 × depth (cm) (r = 0.998) was derived. Thirteen subsequent dates confirm that sedimentation rates for core 2269 are reasonably constant, but reveal that for the purpose of studying sub-millennial timescales, a simple linear model is not appropriate. We have applied several fits to the dates to evaluate the effects of age models on chronologic uncertainty. In Figure 3 we show a fifth-order polynomial and linear interpolation between dates. The polynomial fit, which is a simple expression that retains an assumption of smoothly changing sedimentation rates, does a better job of honoring the dates than would a linear regression for core 2269 [e.g., *Andrews et al.*, 2003]. A fifth-order polynomial fit is reasonable for core 2322 as it tracks the large change in sedimentation rate at about 9 ka. Linear interpolation between dates (assuming a constant sedimentation rate between successive dates) respects all of the data, but forces sedimentation rate changes to occur at dated intervals. For core 2269, the difference between the fits is surprising and exceeds 400 years in one instance (Figure 3b). For core 2322, the differences between the two age models are less pronounced (Figure 3b).

4.1.2. Core Top and Basal Ages

[12] The core top date for core 2269 is 72 ± 37 ^{14}C years B.P., consistent with contamination by bomb radiocarbon and that the core top sediments are <50 years old. The core top date for core 2322 is 675 ± 30 ^{14}C years B.P. with a $1-\sigma$ calibration to 277, 322, 360 cal years B.P. Both cores have basal radiocarbon dates obtained from the core catcher. These dates are; for 2269, 10920 ± 85 ^{14}C years B.P., which

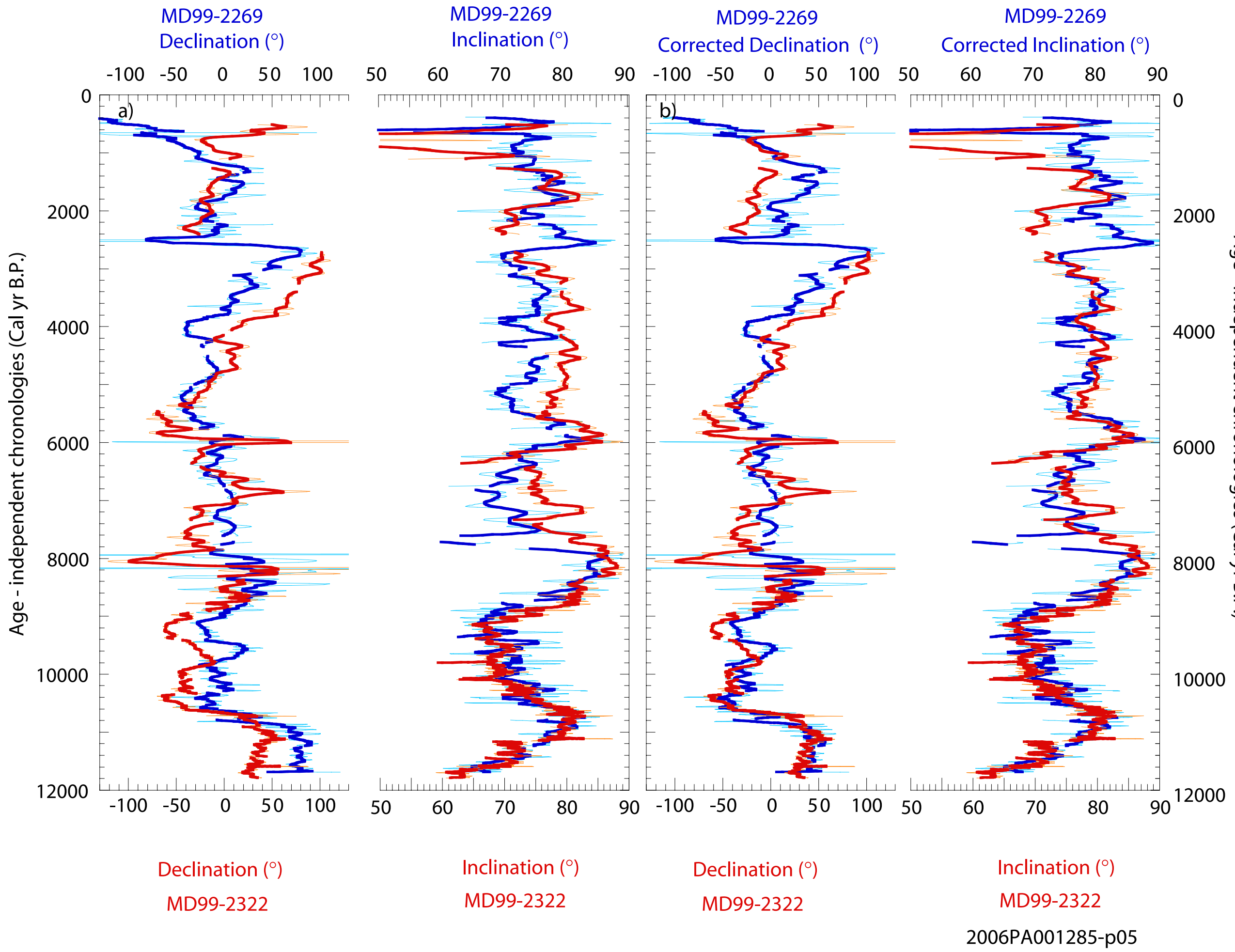

Figure 5. (a) Comparison of paleomagnetic secular variation for the studied cores on their independent calibrated radiocarbon chronologies as defined from the linear interpolation age models in Figure 3. (left) ChRM declination comparison between cores MD99-2269 (blue) and MD99-2322 (red), with r = 0.450 (0.552) before (after) smoothing. (right) ChRM inclination comparison between MD99-2269 (blue) and MD99-2322 (red), with r = 0.39 (0.463) before and (after) smoothing. (b) Comparison of PSV on the independent chronologies after correcting core MD99-2269 for minor coring artifacts. These include subtracting a linear trend in the core 2269 declination consistent with a clockwise rotation (3.18°/m) during coring and adding a constant 4° to the core 2269 inclinations (not exceeding 90°) for the upper 1444 cm of the core (see text for discussion). (left) ChRM declination comparison between cores MD99-2269 (blue) and MD99-2322 (red), with r = 0.56 (0.689) before (after) smoothing. (right) ChRM inclination comparison between cores MD99-2269 (blue) and MD99-2322 (red), with r = 0.461 (0.529) before (after) smoothing.

calibrates using the full $1-\sigma$ range to 12351, 12489, 12672 cal years B.P. and for core 2322, 11125 ± 80 ^{14}C years B.P., with a $1-\sigma$ calibration to 12707, 12765, 12835 cal years B.P. (Table 1).

[13] The basal ages of both cores were obtained from core catcher samples. As more dates from the cores were obtained, the core catcher ages appeared to be older than would be expected relative to the overlying dates (Figure 3). The core catcher dates could be further evaluated by comparison with the occurrence of the Younger Dryas marker, the Vedde Ash [*Grönvold et al.*, 1995]. Vedde Ash shards were observed and identified by geochemical analyses (by K. Grönvold, Nordic Volcanological Institute) in the core catchers of both cores. The Vedde Ash was not, however, cored in either record. Therefore its initial occurrence was not sampled and the age of the Vedde Ash represents a maximum age for the base of both cores. Chronological estimates for the Vedde Ash based on radiocarbon dated lake sediments are 10330 ± 50 ^{14}C years B.P. [*Birks et al.*, 1996] with a $1-\sigma$ calibration to 12050, 12168, 12239 capturing 98.5% of the range [*Reimer et al.*, 2004]. In the Greenland Summit GRIP ice core, Vedde Ash was found at a depth of 1639.54 m with an age estimate of 11980 ± 80 cal years B.P. [*Grönvold et al.*, 1995] using the

Table 2. Radiocarbon and PSV Tie Points for the Studied Cores

	Core MD99-2322 Radiocarbon Dates				Depth Equivalent in MD99-2269			
		2322 Calibrated Ages			Depths Based on Age Model in Figure 3			
	Depth of Radiocarbon Dates, cm	Minimum 1 σ, cal years B.P.	Median Probability, cal years B.P.	Maximum 1σ, cal years B.P.	Minimum 1 σ, cm	Median Probability, cm	Maximum 1 σ, cm	Depth Based on PSV Correlation,[a] cm
MD99-2322	2.5	277	322	360	37	42	53	
MD99-2322	34	290	344	385	38	48	62	
MD99-2322	101.5	761	812	875	177	188	201	
MD99-2322	150	1146	1191	1250	253	259	266	250
MD99-2322	368	3280	3332	3381	628	636	643	633
MD99-2322	564	5125	5213	5299	1057	1075	1092	1075
MD99-2322	771	6467	6545	6626	1294	1303	1313	1309
MD99-2322	1073	8170	8522	8883	1512	1565	1638	1564
MD99-2322	1298	9189	9272	9385	1702	1725	1760	1711
MD99-2322	1393	9466	9535	9595	1786	1807	1826	1775
MD99-2322	1432	9552	9679	9755	1813	1853	1877	1806
MD99-2322	1516	9716	9859	9999	1864	1909	1953	1860
MD99-2322	1807	10273	10369	10466	2046	2078	2109	2085
MD99-2322	1908	10519	10616	10692	2126	2157	2181	2154
MD99-2322	2006	10567	10675	10751	2141	2175	2199	2199
MD99-2322	2140	10921	11017	11143	2253	2283	2323	2270
MD99-2322	2342	11180	11296	11375	2335	2371	2396	2399
MD99-2322	2436	11345	11547	11706	2387	2451	2501	2503
MD99-2322	2542	11365	11621	11851	2393	2474	2547	2542
Basal age estimate[b]	2617		11850			2531		2620

	Core MD99-2269 Radiocarbon Dates				Depth Equivalent in Core MD99-2322			
		2269 Calibrated Ages			Depths Based on Age Model in Figure 3			
	Depth of Radiocarbon Dates, cm	Minimum 1 σ, cal years B.P.	Median Probability, cal years B.P.	Maximum 1 σ, cal years B.P.	Minimum 1 σ, cm	Median Probability, cm	Maximum 1 σ, cm	Depth Based on PSV Correlation,[a] cm
MD99-2269	1		0					
MD99-2269	42.5	281	328	364	−56	11	37	
MD99-2269	131	556	590	623	65	69	74	
MD99-2269	161	644	679	711	77	82	87	
MD99-2269	177.5	718	762	795	88	94	99	
MD99-2269	246	1036	1091	1161	130	137	146	
MD99-2269	266	1210	1250	1293	152	156	160	159
MD99-2269	351	1489	1536	1593	180	185	191	187
MD99-2269	412	1966	2028	2098	229	235	242	227
MD99-2269	456	2189	2247	2315	252	258	264	258
MD99-2269	563	2741	2787	2824	308	313	316	310
MD99-2269	621	3142	3237	3345	349	358	369	360
MD99-2269	707.5	3730	3793	3845	409	416	421	415
MD99-2269	815	3866	3939	3992	424	431	437	456
MD99-2269	937.5	4407	4474	4527	480	487	493	497
MD99-2269	974	4638	4703	4793	504	511	520	507
MD99-2269	1162	5592	5657	5704	623	633	640	644
MD99-2269	1268	6192	6245	6289	716	724	731	719
MD99-2269	1398	7274	7351	7419	882	894	905	853
MD99-2269	1519.5	8159	8222	8298	1018	1027	1039	1017
MD99-2269	1568	8458	8545	8608	1063	1080	1099	1079
MD99-2269	1708	9106	9219	9330	1248	1282	1319	1294
MD99-2269	1718	9162	9251	9325	1265	1292	1317	1308
MD99-2269	1980.5	9966	10085	10193	1577	1645	1707	1685
MD99-2269	2068	10227	10336	10425	1726	1788	1830	1780
Basal age estimate[b]	2499		11700			2574		2431

[a]Defined in Figures 6 and 7.
[b]Based on linear interpolated age model in Figure 3.

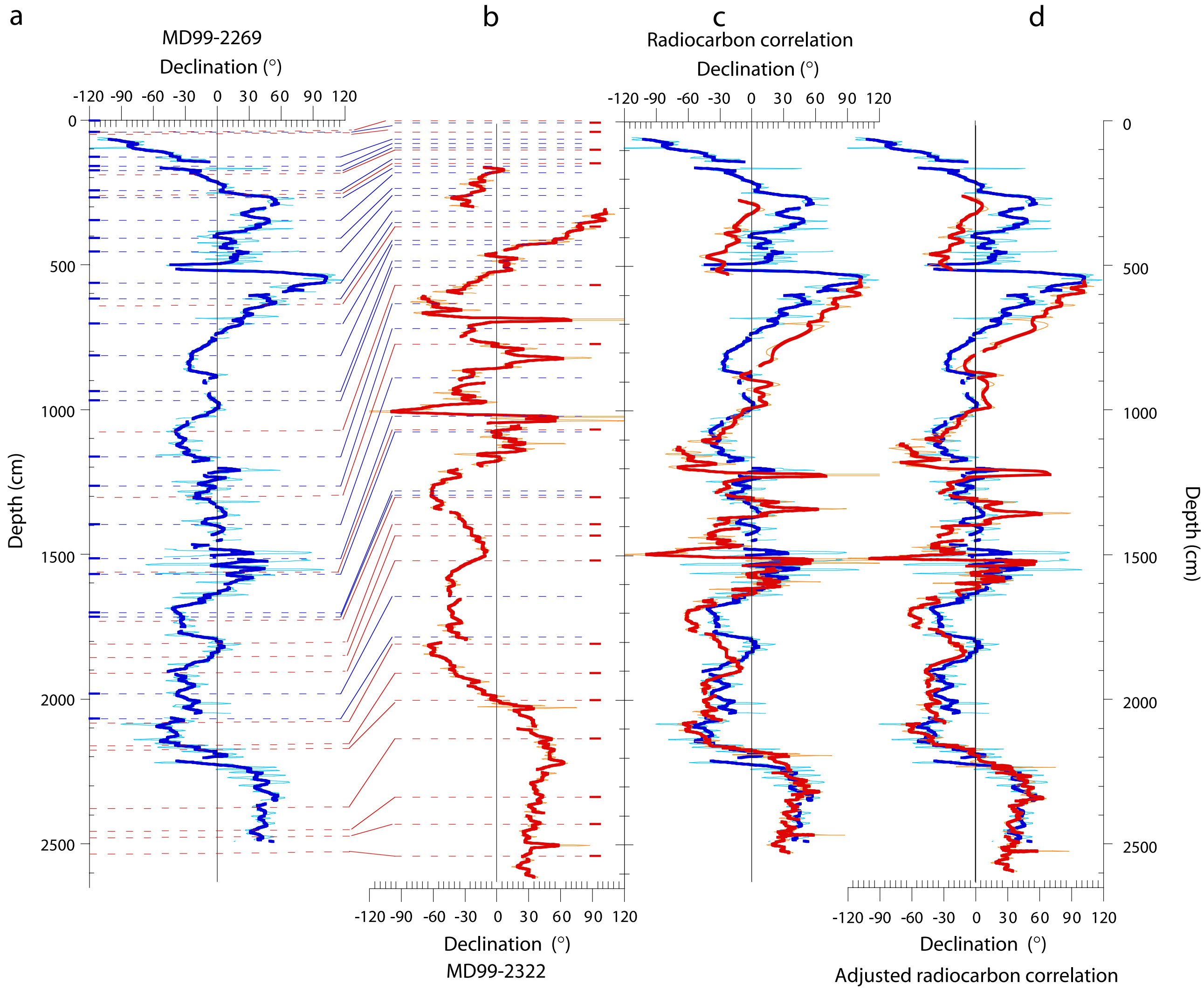

Figure 6. Declination comparison of PSV records for cores (a) MD99-2269 (blue) and (b) MD99-2322 (red) versus depth. Blue (red) bars indicate position of core 2269 (2322) radiocarbon dates. Dashed blue (red) lines show core 2269 (2322) tie points based on the position of the radiocarbon dates that are linked to the corresponding position in the opposing core based on the linearly interpolated age model in Figure 3. (c) Results of a tie point correlation of declination by adjusting the depth of core 2322 (red) to those of core 2269 (blue), with r = 0.612 (0.692) before (after) smoothing. (d) Results using the Analyseries program [*Paillard et al.*, 1996], adjusting the depths of the declination and inclination records by moving or creating new tie points to improve the correlation, with r = 0.699 (0.758) for declination before (after) smoothing.

SS09 chronology [*Johnsen et al.*, 1995]. Although no published age exists for the Vedde Ash in the nearby GISP2 ice core, relative correlations between the two records indicate that the official chronology for GISP2 [*Meese et al.*, 1997; *Sowers et al.*, 1993] is ~100 years older than the GRIP SS09 chronology [*Mogensen*, 2001] during this part of the Younger Dryas. The older age estimate is more in line with the calibration of the *Birks et al.* [1996] radiocarbon age. On the basis of the geochemical identification of the Vedde Ash (K. Grönvold, personal communication, 2005) in the core catcher and basal sediments of both cores, the basal age should not be much older than ~12,000 cal years B.P. and is therefore discrepant with the calibrated radiocarbon ages derived from the basal dates.

[14] Radiocarbon-based sedimentation rate estimates (excluding the core catcher dates) provide another approach to evaluate the discrepancy between the core catcher dates and the occurrence of Vedde Ash. At a depth of 2541–2543 cm, which is only 94 cm from the base of core 2322 (Table 1), an abundance spike of the benthic foraminferal species *Islandiella norcrossi*, augmented by several other species, provided the lowest level from which a high-quality radiocarbon date could be obtained. An additional six radiocarbon dates from the lower 7 m of core 2322 were acquired. Core 2269, on the other hand, has little carbonate

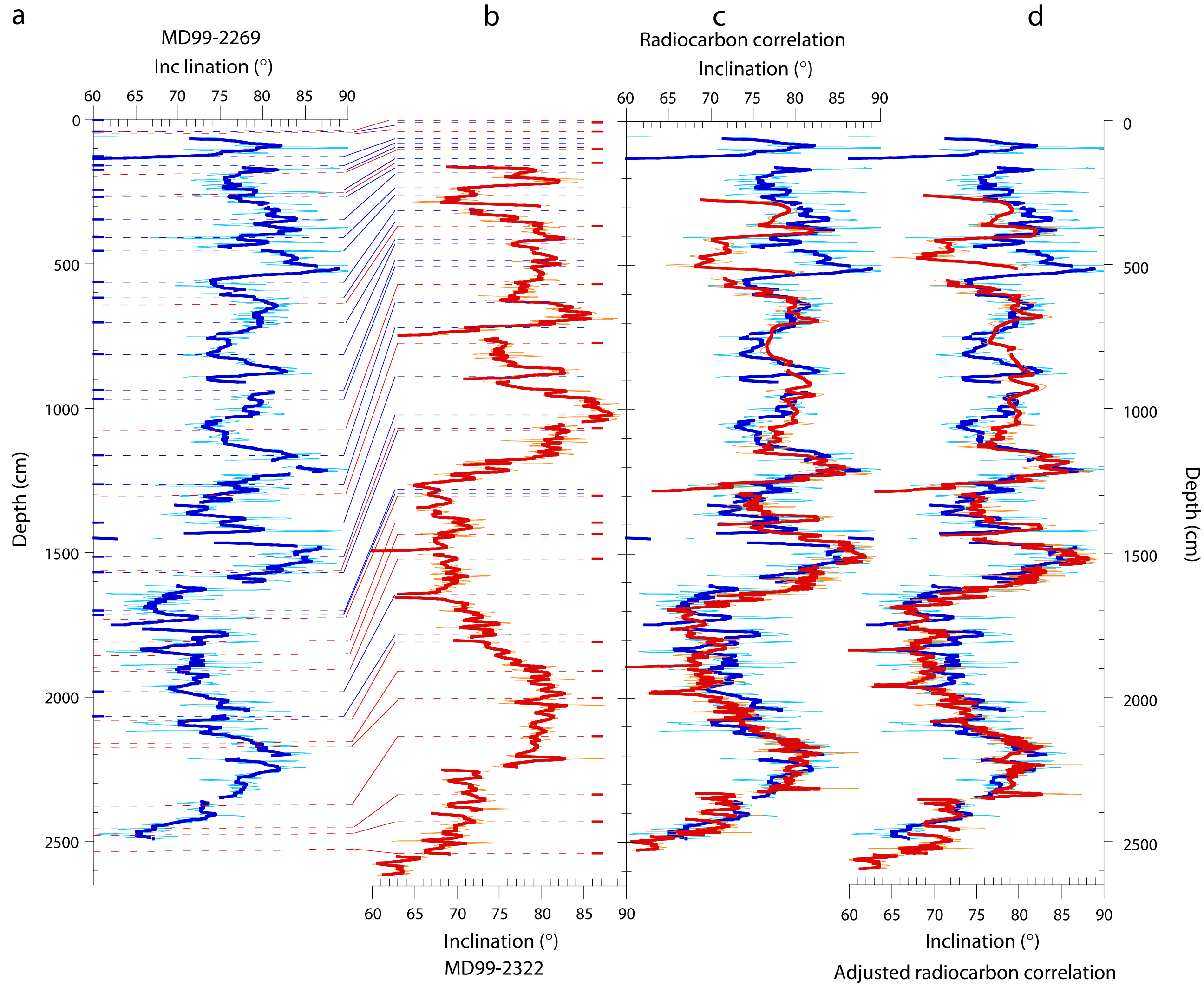

Figure 7. Inclination comparison of PSV records for cores (a) 2269 (blue) and (b) 2322 (red) versus depth. Blue (red) bars indicate position of core 2269 (2322) radiocarbon dates. Dashed blue (red) lines show core 2269 (2322) tie points based on the position of the radiocarbon dates which are linked to the corresponding position in the opposing core based on the linearly interpolated age model in Figure 3. (c) Results of a tie point correlation of inclination by adjusting the depth of core 2322 (red) to those of core 2269 (blue), with r = 0.468 (0.571) before and (after) smoothing. (d) Results using the Analyseries program [*Paillard et al.*, 1996], adjusting the depths of the declination and inclination records by moving or creating new tie points to improve the correlation, with r = 0.629 (0.711) for inclination before (after) smoothing.

material to constrain the basal age. The deepest radiocarbon date in 2269 occurs at 2068 cm, more than 4 m from the base. Using the lowest seven dates in core 2322 (Table 1) and projecting a constant sedimentation rate (577 cm/kyr, $r^2 = 0.989$) provides a basal age estimate of ca 11850 years. Using the lowest four dates from core 2269 and assuming a constant linear sedimentation rate (315 cm/kyr, $r^2 = 0.999$) through the undated lower 4 m of the core provides a basal age estimate of 11700 years. These estimates are consistent with the observation of Vedde Ash in the core catchers. For the core catcher basal radiocarbon ages to be correct, not only would we have to disregard the observation of the Vedde Ash, but especially for core 2322, we would have to invoke an implausible near cessation of sedimentation at that site. Consequently, we eliminate the anomalously old ages obtained from the core catchers from our age models (Figure 3).

[15] One explanation for the basal dates being apparently too old is that they were affected by a larger marine reservoir correction (∼500 years for core 2269 and ∼750 years for core 2322) during the Younger Dryas cold period. Anomalously high and variable reservoir corrections have been reconstructed during this time in the North Atlantic and Nordic Seas [i.e., *Bard et al.*, 1994; *Austin et*

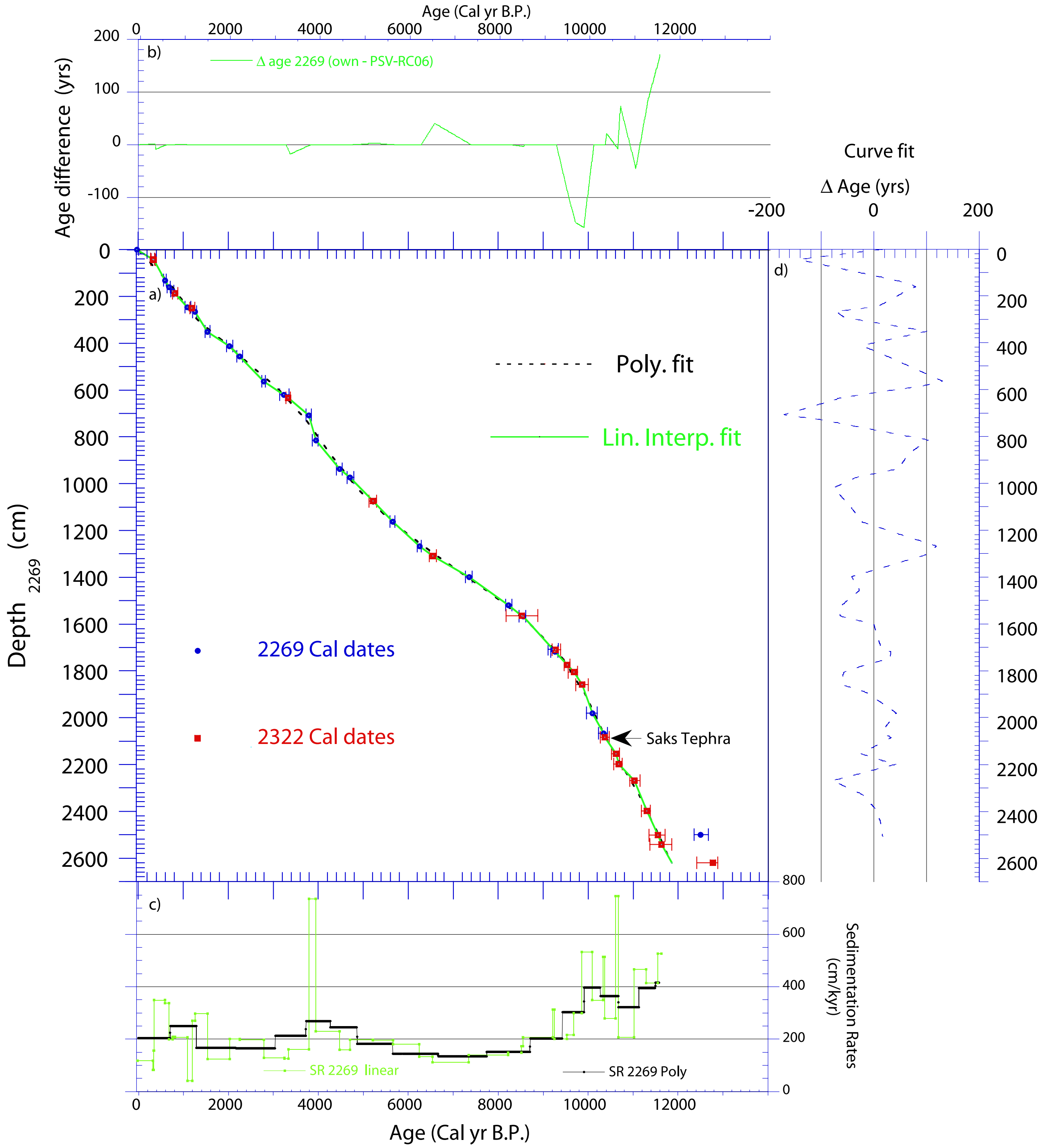

Figure 8. Commingled calibrated radiocarbon dates plotted on depth for core MD99-2269. (a) Commingled calibrated radiocarbon dates for cores MD99-2269 (blue) and MD99-2322 (red) (Table 3) and associated age models based on linear interpolation between dates and a ninth-order polynomial on a common core 2269 depth scale as derived by the PSV correlation shown in Figures 6 and 7. Error bars on dates equal $1 - \sigma$ calibrated age ranges. (b) Age difference between the core 2269 independent chronology (Figure 3) and the PSV-RC06 chronology based on the linear interpolation between dates. (c) Sedimentation rates for core 2269 based on linear interpolation between dates (green) and on the ninth-order polynomial fit (black). (d) Age difference between linear interpolation and the ninth-order polynomial fit to the dates. A positive (negative) age difference at any depth means that the polynomial fit is older (younger).

al., 1995; *Björck et al.*, 2003]. However, prior work on cores from the Kangerlussuaq Trough that extend through both the Vedde Ash and the Younger Dryas do not support an increased reservoir correction [*Jennings et al.*, 2002, 2006]. Therefore, at least in core 2322, other sources of older carbon should be considered. Reworked foraminifera included in the dated mixed assemblage or sampling of deeper sediments by the core catcher through overpenetration after the core barrel was filled [e.g., *Skinner and McCave*, 2003] are possibilities.

4.2. Paleomagnetic Results From Cores 2269 and 2322

4.2.1. Natural Remanent Magnetization

[16] The natural remanent magnetization (NRM) of these homogenous sediments for both 2269 and 2322 is strong and stable throughout the entire sequence (Figure 4). The NRM intensities prior to demagnetization range from

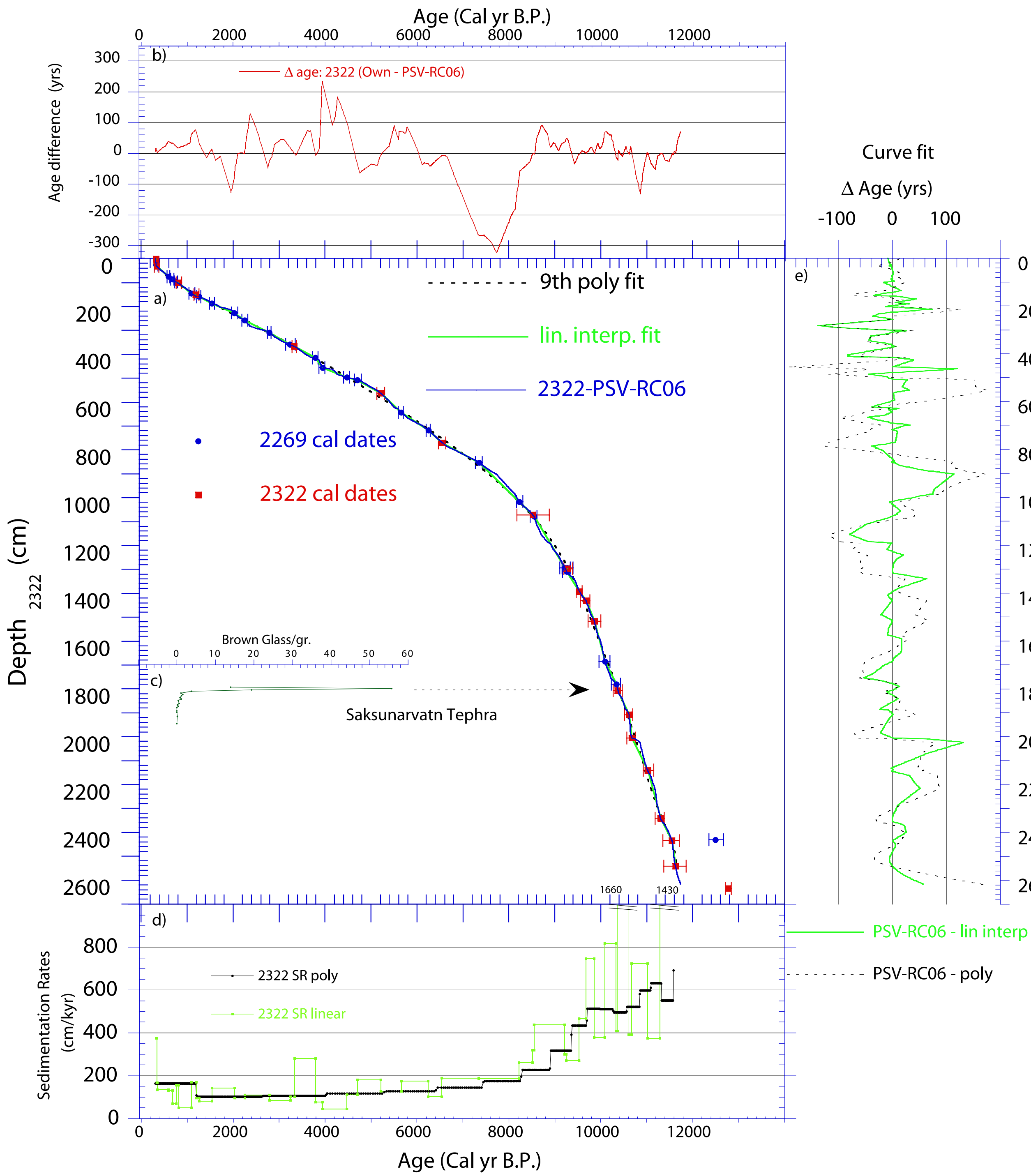

Figure 9

Table 3. Table of Dates in Figures 8 and 9 Used to Construct the PSV-RC06 Age Models in Figure 10

	Depths of Radiocarbon Dates									
	MD99-2269		MD99-2232		Commingled Dates					
Core	2269 Depths,[a] cm	2322 Depths (PSV), cm	2322 Depths, cm	2269 Depths, (PSV),[a] cm	2269 Depths, cm[a]	2322 Depths, cm	Reported Age, ^{14}C years B.P.	Minimum 1 σ, cal years B.P.	Median Probability,[b] cal years B.P.	Maximum 1 σ, cal years B.P.
MD99-2269	1				1		72 ± 37		−30[c]	
MD99-2322			2.5	42	42	2.5	675 ± 30	277	322	360
MD99-2269	42.5	28			42.5	28	680 ± 30	281	328	364
MD99-2322			34	45	45	34	693 ± 38	290	344	385
MD99-2269	131	75			131	75	1010 ± 30	556	590	623
MD99-2269	161	87			161	87	1124 ± 41	644	679	711
MD99-2269	177.5	98			177.5	98	1226 ± 25	718	762	795
MD99-2322			101.5	188	188	101.5	1267 ± 44	761	812	875
MD99-2269	246	145			246	145	1535 ± 47	1036	1091	1161
MD99-2322			150	250	250	150	1627 ± 46	1146	1191	1250
MD99-2269	266	160			266	160	1693 ± 42	1210	1250	1293
MD99-2269	351	187			351	187	1978 ± 35	1489	1536	1593
MD99-2269	412	227			412	227	2396 ± 47	1966	2028	2098
MD99-2269	456	258			456	258	2578 ± 48	2189	2247	2315
MD99-2269	563	310			563	310	3017 ± 39	2741	2787	2824
MD99-2269	621	360			621	360	3375 ± 80	3142	3237	3345
MD99-2322			368	633	633	368	3451 ± 39	3280	3332	3381
MD99-2269	707.5	415			707.5	415	3840 ± 33	3730	3793	3845
MD99-2269	815	456			815	456	3949 ± 39	3866	3939	3992
MD99-2269	937.5	497			937.5	497	4340 ± 46	4407	4474	4527
MD99-2269	974	507			974	507	4505 ± 50	4638	4703	4793
MD99-2322			564	1075	1075	564	4899 ± 55	5125	5213	5299
MD99-2269	1162	644			1162	644	5296 ± 53	5592	5657	5704
MD99-2269	1268	719			1268	719	5826 ± 51	6192	6245	6289
MD99-2322			771	1308	1308	771	6115 ± 65	6467	6545	6626
MD99-2269	1398	853			1398	853	6833 ± 81	7274	7351	7419
MD99-2269	1519.5	1017			1519.5	1017	7749 ± 62	8159	8222	8298
MD99-2322			1073	1564	1564	1073	8000 ± 300	8170	8522	8883
MD99-2269	1568	1079			1568	1079	8084 ± 57	8458	8545	8608
MD99-2269	1708	1294			1708	1294	8572 ± 78	9106	9219	9330
MD99-2322			1298	1710	1710	1298	8609 ± 67	9189	9272	9385
MD99-2269	1718	1308			1718	1308	8590 ± 43	9162	9251	9325
MD99-2322			1393	1775	1775	1393	8877 ± 62	9466	9535	9595
MD99-2322			1432	1806	1806	1432	8999 ± 61	9552	9679	9755
MD99-2322			1516	1860	1860	1516	9108 ± 65	9716	9859	9999
MD99-2269	1980.5	1685			1980.5	1685	9265 ± 70	9966	10085	10193
MD99-2269	2068	1780			2068	1780	9477 ± 88	10227	10336	10425
MD99-2322			1807	2085	2085	1807	9514 ± 81	10273	10369	10466
MD99-2322			1908	2154	2154	1908	9747 ± 76	10519	10616	10692
MD99-2322			2006	2198	2198	2006	9803 ± 64	10567	10675	10751
MD99-2322			2140	2269	2269	2140	10,034 ± 69	10921	11017	11143
MD99-2322			2342	2399	2399	2342	10,293 ± 77	11180	11296	11375
MD99-2322			2436	2503	2503	2436	10,442 ± 82	11345	11547	11706
MD99-2322			2542	2542	2542	2542	10,480 ± 110	11365	11621	11851

[a]Gap-corrected depths.
[b]Calibrated using Calib 5.0 [*Stuiver and Reimer*, 1993] and the updated marine calibration data sets [*Hughen et al.*, 2004].
[c]Age estimate.

Figure 9. Commingled calibrated radiocarbon dates plotted on depth for core MD99-2322. (a) Commingled calibrated radiocarbon dates for cores MD99-2269 (blue) and MD99-2322 (red) (Tables 2 and 3) and associated age models based on linear interpolation between dates (green), ninth-order polynomial (dashed) and PSV-RC06 chronology on the core 2322 depth scale as derived by the PSV correlation shown in Figures 6 and 7. Error bars on dates indicate maximum spread of all $1 - \sigma$ calibrated age ranges. (b) Age difference between the core 2322 independent chronology (Figure 3) and the PSV-RC06 chronology (Figure 8) transferred to core 2322 depths using PSV correlation (Figures 6 and 7). (c) Grain counts showing maximum abundance of brown volcanic glass at 1797.5 cm, which has been verified as Saksunarvatn tephra by geochemical analyses (by K. Grönvold, Nordic Volcanological Institute). (d) Sedimentation rates for core 2322 based on linear interpolation between dates (green) and on the ninth-order polynomial fit (black). (e) Age difference between the PSV-RC06 chronology and linear interpolation (green) and ninth-order polynomial (dashed) fits to the dates on the core 2322 depth scale. A positive (negative) age difference at any depth means that the linear interpolation or polynomial fit is older (younger).

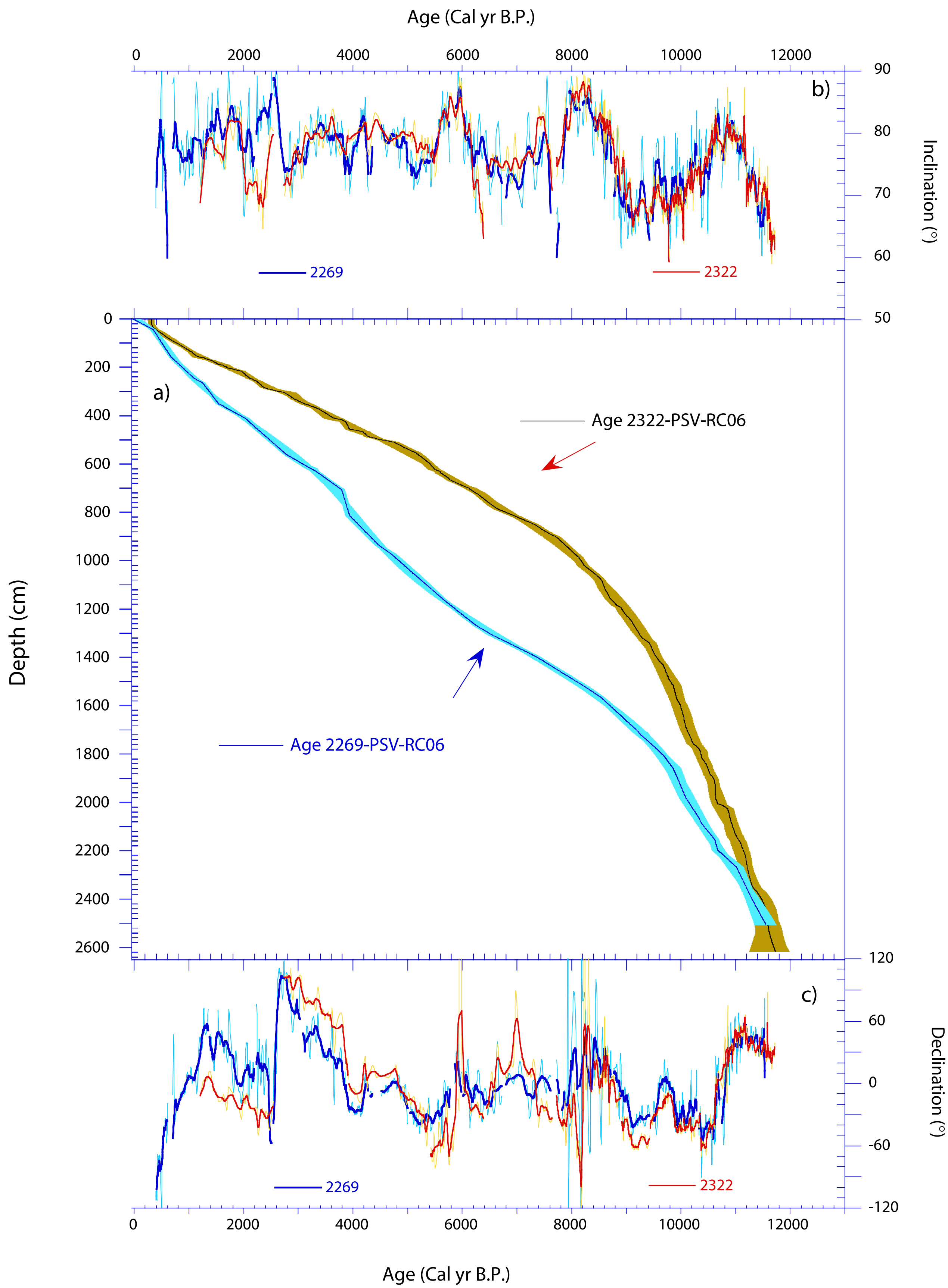

Age (Cal yr B.P.)
0
2000
4000
6000
8000
10000
12000
b)
90
80
70
60
50
Inclination (°)
2269
2322
a)
Depth (cm)
0
200
400
600
800
1000
1200
1400
1600
1800
2000
2200
2400
2600
Age 2322-PSV-RC06
Age 2269-PSV-RC06
120
c)
60
0
-60
-120
Declination (°)
2269
2322
0
2000
4000
6000
8000
10000
12000
Age (Cal yr B.P.)

Figure 10

~0.1 to 0.6 A/m. AF demagnetization data reveal a stable single component magnetization that is directed toward the origin of the vector component diagram. Less than 20% of the initial NRM remains after AF demagnetization at 60 mT and the median destructive field (MDF) varies between 20 and 30 mT. This strong, low coercivity magnetization is consistent with magnetite or titanomagnetite as the remanence carrier, as expected from the glacial erosion of basaltic bedrock in east Greenland [*Brooks*, 1990] and Iceland [*Einarsson*, 1973]. Paleomagnetic directions were calculated by principal component analysis [*Kirschvink*, 1980] using 5 or 6 consecutive AF demagnetization steps at peak fields between 10 and 60 mT. Maximum angular deviation (MAD) values of the calculated best fit characteristic remanent magnetization (ChRM) are often less than 1° (Figure 4), which attests to the quality of the data. ChRM inclinations for both cores vary around the expected geocentric axial dipole inclination (~78°) at the latitudes of these sites (Figure 4). Though independent azimuthal control was not available during coring, the cores were split on a constant plane with the relative ChRM declinations (Figure 4) rotated to an entire core mean of zero (Figure 5). The assumption of a zero mean declination is reasonable considering that almost 12,000 years of geomagnetic behavior is being averaged [e.g., *Merrill and McFadden*, 2003]. Relative declinations should therefore approximate absolute changes. Overall, the magnetic properties and paleomagnetic behavior are optimal for reconstructing past directional changes of the Earth's magnetic field. The geomagnetic implications of these records will be presented elsewhere (J. S. Stoner et al., Holocene paleomagnetic secular variation controlled by persistent high-latitude locations of varying geomagnetic flux, manuscript in preparation, 2006).

4.2.2. Paleomagnetic Secular Variation Records From Cores 2322 and 2269

[17] In Figure 5, the PSV (declination and inclination) records for cores 2322 and 2269 are presented on age models derived from linear interpolation of the calibrated AMS ^{14}C dates with the basal age constrained by constant sedimentation rates as described above (Figure 3). Because of the high sediment accumulation rates at these sites, high-frequency centennial-scale variations are superimposed on longer-term directional changes more typically associated with PSV records [e.g., *Turner and Thompson*, 1981; *Thompson*, 1984; *Lund*, 1996]. The higher-frequency variations are comparable with historical secular variation (HSV) in both amplitude and period at the site locations [e.g., *Jackson et al.*, 2000]. HSV has rarely been captured in sediment records, with the high-resolution sediments of the Aral Sea providing one of the few other examples [*Nourgaliev et al.*, 2003]. The amplitude and rates of change of longer period PSV are also high when compared to records at similar latitudes from Scandinavia [e.g., *Ojala and Tiljander*, 2003; *Snowball and Sandgren*, 2002, 2004]. Suggesting that the high temporal resolution of these cores preserve a more complete, less smoothed, geomagnetic record. For purposes of comparison and correlation, we present the original data before and after smoothing; 20 cm for core 2269 and 10-cm smoothing for core 2322, providing a ~100- year running mean for the upper part of each record (Figure 5).

[18] Declination and inclination records from cores 2322 and 2269 are similar to one another (Figure 5a). Differences that occur are often found in areas where soft sediment deformation is likely, such as core tops, section breaks, and sediments adjacent to voids. Disregarding the shallow inclinations observed at the top of both cores and all of section I of core 2322, likely resulting from soft sediment deformation, the correlations of the PSV records on their own independent timescales (e.g., Figure 3) are r = 0.450 (0.552) before (after) smoothing for declination (Figure 5a, left panel) and r = 0.39 (0.463) for inclination (Figure 5a, right panel). Inclinations in core 2269, although similar in pattern, are shallow by ~4° for the upper ~8000 cal years B.P. (upper 1444 cm) compared to those from core 2322 (Figure 5). Below this depth, shallow inclinations in core 2269 are not apparent. Declinations in core 2269 display a linear trend not apparent in the core 2322 declination record (Figure 4b). The trend is consistent with a 3.18°/m clockwise rotation during coring. Simply adding 4° (not exceeding 90°) to the inclinations of the upper 1444 cm of core 2269 and subtracting the linear trend in declination, significantly improves the correlation to r = 0.56 (0.689) for declination (Figure 5b, right panel) and r = 0.461 (0.529) for inclination before and (after) smoothing (Figure 5b, left panel). It should be noted that the interval of shallow inclination in core 2269 (upper 1444 cm) corresponds to, and ends at, the 3rd or deepest void (noted earlier) found in the core. Core stretching associated with the *Marion Dufresne II* Calypso coring system is a well-known, though sporadic, process that is generally restricted to the upper 10 to 15 m of affected cores [*Turon and Hillaire-Marcel*, 1999; *Thouveny et al.*, 2000; *Skinner and McCave*, 2003]. These cores show no evidence of stretching-induced accumulation rate gains, as demonstrated by comparison between the core depth of the Saksunarvatn Tephra in core 2269 and its depth as a major reflector in acoustic profiles [*Andrews et al.*, 2003]. We suspect that coring stresses were mostly taken up by void formation at tephra (coarser and weaker) layers. This has mitigated core stretching, but it may have slightly affected the inclination record, resulting in subtle inclination shallowing. Although significant stretching can compromise paleomagnetic records [*Thouveny et al.*, 2000] and result in dramatic apparent accumulation rate changes [*Turon and Hillaire-Marcel*, 1999], such problems were apparently avoided in core 2269 by void formation.

Figure 10. PSV-RC06 age models and PSV records for cores MD99-2269 and MD99-2322. (a) PSV-RC06 age models for cores 2269 and 2322 with associated $1-\sigma$ uncertainty envelopes. (b) Inclination records (Figure 5b) from cores 2269 (blue) and 2322 (red) on the PSV-RC06 chronology. (c) Declination records (Figure 5b) from cores 2269 (blue) and 2322 (red) on the PSV-RC06 chronology.

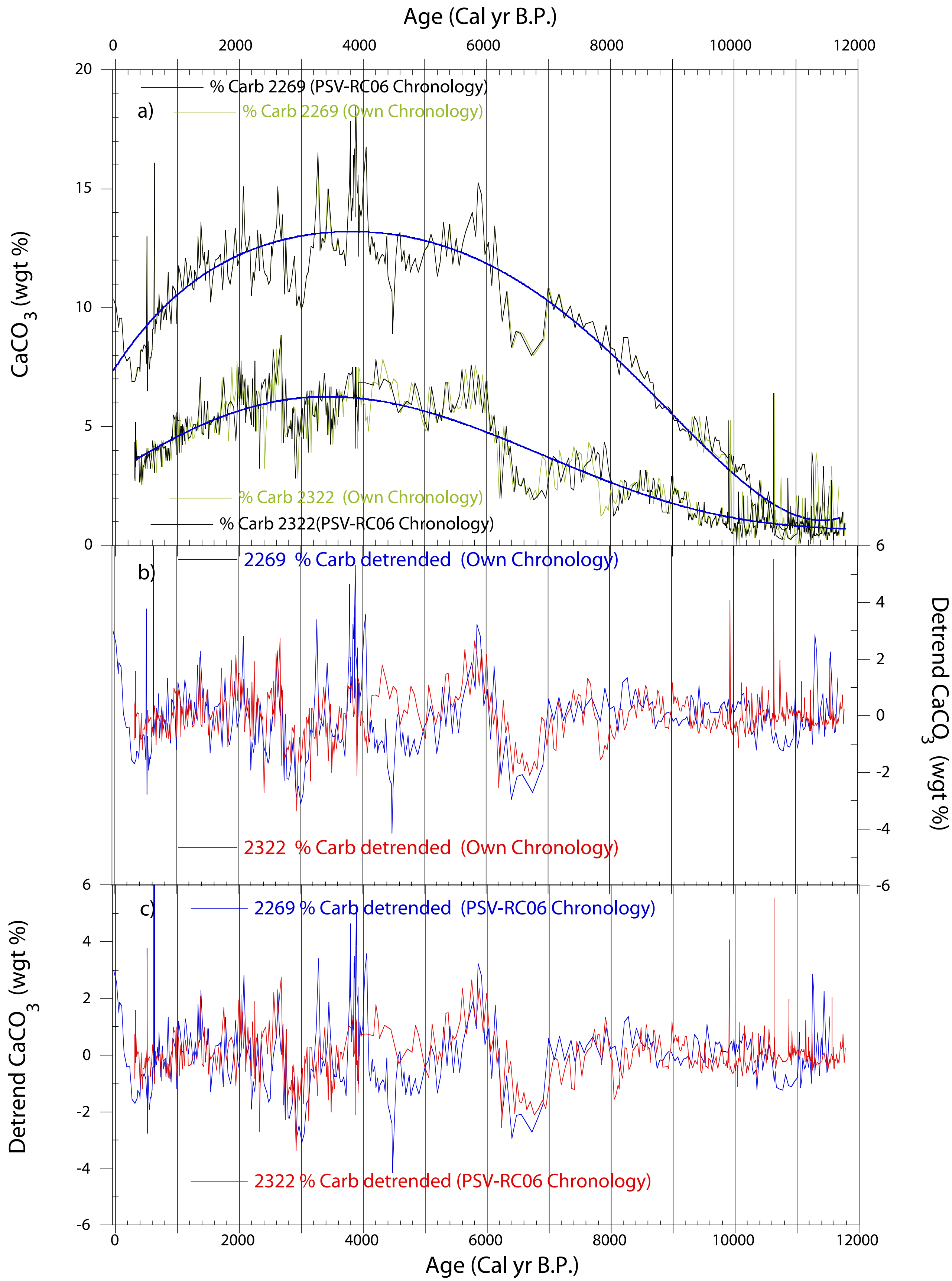
Age (Cal yr B.P.)
0
2000
4000
6000
8000
10000
12000
20
15
10
5
0
CaCO3 (wgt %)
a)
% Carb 2269 (PSV-RC06 Chronology)
% Carb 2269 (Own Chronology)
% Carb 2322 (Own Chronology)
% Carb 2322(PSV-RC06 Chronology)
b)
2269 % Carb detrended (Own Chronology)
2322 % Carb detrended (Own Chronology)
6
4
2
0
-2
-4
-6
Detrend CaCO3 (wgt %)
c)
2269 % Carb detrended (PSV-RC06 Chronology)
2322 % Carb detrended (PSV-RC06 Chronology)
Detrend CaCO3 (wgt %)
Age (Cal yr B.P.)

Figure 11

4.3. Developing a PSV-Radiocarbon Age/Depth Model for Cores 2269 and 2322

[19] In the previous section, it was shown that PSV from cores 2269 and 2322 are similar on their independent radiocarbon timescales (Figure 5). Historical (~400 years) reconstructions show that patterns of secular variation at these locations are essentially identical for the last 400 years [*Jackson et al.*, 2000]. It is therefore reasonable to assume that longer period variations should have also been essentially identical as they likely reflect geomagnetic features of even larger spatial scale [e.g., *Lund*, 1996; *Constable et al.*, 2000; *Korte and Constable*, 2005]. The premise behind PSV correlation or dating is based on this regional similarity. Tests of PSV synchronization of lake sediments in Finland demonstrate that PSV correlations at distinct tie points can be made within varve-based chronological uncertainties (~1%) for much of the Holocene [*Ojala and Tiljander*, 2003]. The utility of the method and its uncertainties in marine sediments has not, however, been tested. The independent chronologies reported here clearly support the use of PSV as a chronostratigraphic tool (Figure 5). The question is, can PSV improve already strong radiocarbon chronologies as well as provide chronological control when dates are less common? The chronologies presented here are of high quality (Figure 3 and Table 1) but have enough uncertainties (Figure 3b) that centennial-scale relationships remain ambiguous (Figure 2).

4.3.1. PSV Correlations in the Depth Domain

[20] To improve not only the relative correlation between the two records, but also the overall chronology, the PSV records are first correlated in the depth domain. The radiocarbon dates provide initial tie points (Figure 3 and Table 2). These are derived by calculating the depth equivalents of each date in the opposing core using the linear interpolated age models in Figure 3. For example, the radiocarbon date at 563 cm in core 2269 has a median probability age of 2787 cal years B.P. with a 1 σ range of 2741 to 2824 cal years B.P. (Table 1). Using the linear interpolation age model for core 2322 in Figure 3, a depth equivalent of 2787 cal years B.P. in core 2322 is 313 cm, with a range from 308 to 316 cm (Table 2). This procedure was followed for all dates in cores 2269 and 2322 providing a series of depth-to-depth tie points (Figure 6). PSV correlations in the depth domain using these tie points are r = 0.612 (0.692) for declination (Figure 6c) and r = 0.468 (0.571) for inclination (Figure 7c), before (after) smoothing. Using the Analyseries program [*Paillard et al.*, 1996] the depths of the inclination and declination records are adjusted by moving or creating new tie points to improve the correlation (Table 2). This results in r = 0.699 (0.758) for declination (Figure 6d) and r = 0.629 (0.711) for inclination (Figure 7d), before and (after) smoothing.

[21] The depth-to-depth correlation of cores 2269 and 2322 is supported by the improved correlation of the PSV records, and, as will be discussed below, the consistent interweaving of radiocarbon dates, the correct alignment of the Saksunarvatn tephra (Figures 8 and 9) and the improved correlation of weight percent $CaCO_3$. Unlike core 2269 where the Saksunarvatn tephra occurs as a discrete visible layer between 2085–2088 cm [*Andrews et al.*, 2002; *Kristjánsdóttir et al.*, 2007], in core 2322 it is found as a cryptotephra (nonvisible tephra layer). Using initial PSV correlations, the Saksunarvatn tephra was predicted to be found at ~1800 cm in core 2322. Detailed grain counts located the maximum tephra abundance at 1797.5 cm (Figure 9c), which was verified as the Saksunarvatn tephra by geochemical analyses (by K. Grönvold, Nordic Volcanological Institute).

[22] Changes to the initial radiocarbon-based tie points that result from the PSV correlation are shown in Table 2. In most cases, these changes are within the $1 - \sigma$ age uncertainty for the radiocarbon dates. Intervals where larger depth adjustments are needed correspond to intervals in the opposing core (the core without the radiocarbon date) that are poorly constrained by dates (Figures 8 and 9), which suggests that age models, not the individual dates (excluding potential reservoir effects) are the largest source of chronological errors [e.g., *Telford et al.*, 2004]. PSV, as shown here, can provide a significant check on a poorly dated record, or even on a poorly constrained (low dating density) interval of a well-dated core.

4.3.2. Developing Age/Depth Models

[23] The PSV correlation of core 2322 to core 2269 provides a common core 2269 depth scale in which 25 dates from core 2269 and 19 dates from core 2322 are commingled to form a common age-to-depth profile (Figure 8a and Table 3). Three dates are excluded from the age model. The two basal dates (discussed above) have been shown clearly to be outliers when compared with the other radiocarbon dates on the PSV correlation (Figure 8a) and one duplicated date in core 2269 at 1708 cm is excluded (Table 1). As a result, 44 dates over approximately 25 m are used to construct an age model that can be applied to both cores through the PSV correlation. The commingled dates are also placed on a common core 2322 depth scale (Figure 9a) and are used to refine estimates of sediment accumulation rates (Figures 8c and 9d). It should be noted that an age model calculated from the radiocarbon dates on core 2322 depths differs slightly from that calculated using the core

Figure 11. (a) Comparison of weight percent calcium carbonate for cores (top) MD99-2269 and (bottom) MD99-2322 on their independent (green) r = 0.89 and PSV-RC06 (black) r = 0.895 chronologies. A fifth-order polynomial fit to the $CaCO_3$ data is shown by the blue lines. (b) Comparison of weight percent calcium carbonate for cores MD99-2269 (blue) and MD99-2322 (red) detrended using the fifth-order polynomial shown in Figure 11a on the independent chronology for each core, with r = 0.346. (c) Comparison of weight percent calcium carbonate for cores MD99-2269 (blue) and MD99-2322 (red) detrended using the fifth-order polynomial shown in Figure 11a on the PSV-RC06 chronologies, with r = 0.385.

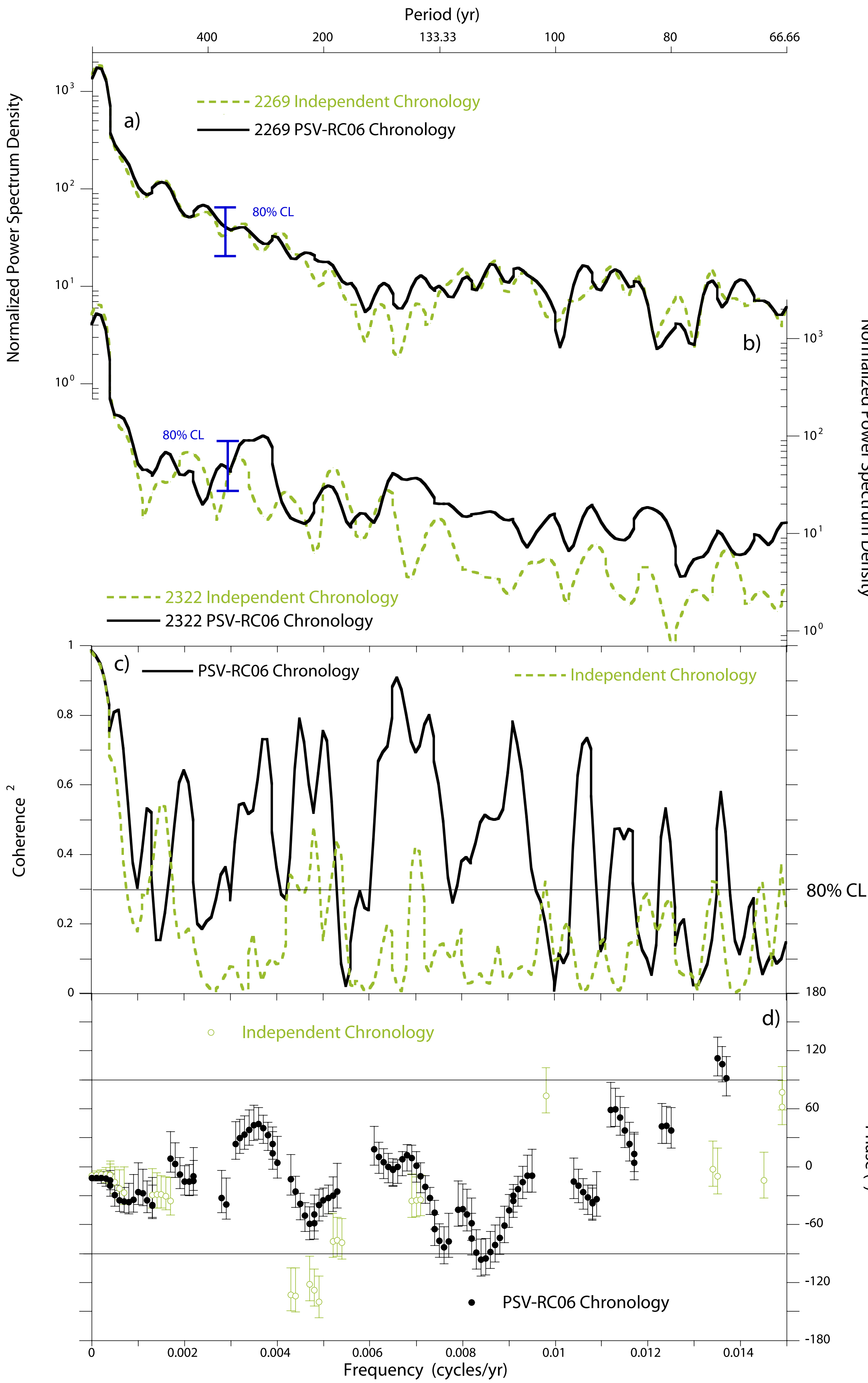

Period (yr)
400
200
133.33
100
80
66.66
a)
2269 Independent Chronology
2269 PSV-RC06 Chronology
80% CL
b)
2322 Independent Chronology
2322 PSV-RC06 Chronology
Normalized Power Spectrum Density
c)
PSV-RC06 Chronology
Independent Chronology
Coherence 2
80% CL
d)
Independent Chronology
PSV-RC06 Chronology
Phase (°)
Frequency (cycles/yr)

Figure 12

2269 depths and transferred to core 2322 depths via the PSV correlation (our preferred method) (Figure 9e).

[24] What is readily apparent and a major test of the reliability of the PSV correlation is the interweaving of radiocarbon dates from both cores on a common core 2269 (Figure 8a) or even core 2322 (Figure 9a) depth scale. Even with this many dates commingled, there is only one stratigraphic inversion of the median probability. A date in core 2322 at 1298 cm (1710 cm_{2269}) of $1-\sigma$ 9189, 9272, 9385 cal years B.P. occurs 8 cm_{2269} above a core 2269 date at 1718 cm_{2269} of 9162, 9251, 9325 cal years B.P. (Table 3). Eight centimeters at this core depth would have been deposited in $\sim$ 40 years (Figure 8c), so that the stratigraphic inversion of the median probability reflects significant overlap of 1σ uncertainties. Such agreement is further illustrated by one of the two 2269 dates at 1708 cm that has the same radiocarbon age as the 2322 date 1710 cm_{2269}. Their different calibrated median probabilities results from their different $1-\sigma$ radiocarbon age precisions (Table 1). Although only a few direct observations are available, they suggest that PSV correlation can, at least in some circumstances, generate synchronization within the inherent uncertainty of radiocarbon dating.

[25] The presentation above indicates that the PSV correlation is robust and the lack of any systematic offsets in radiocarbon dates between the two cores reflects the lack of any significant difference in reservoir ages between these two locations. This does not mean that the reservoir ages have been constant, but that any changes that occurred were generally consistent for these two locations.

5. Discussion

5.1. Commingled Radiocarbon Dates

[26] Comparison between the independent and commingled chronologies for each core indicates that offsets between the linear interpolated age models are small, generally less than 50 (200) years for cores 2269 (2232) and no more than 170 (330) years (Figures 8b and 9b). Chronological differences between the age models occur in intervals where the independent chronology is poorly constrained by radiocarbon dates (Figures 3, 8, and 9). In core 2269 this is most apparent in the lowest 4 m where the few available dates (Figure 3) are augmented by seven core 2322 dates (Figure 8a). This constrains the core 2269 chronology and supports the assumption of consistently high sedimentation rates in the lower part of the record. Only minor chronology changes (<50 years) occur in the upper approximately 9000 years where the dating density of 2269 was already high (Figures 3 and 8b). Reduced age model uncertainty is shown by the increased similarity of the linear interpolated and polynomial fits (Figures 3 and 8d). The better defined age-to-depth relationship allows a higher-order polynomial (ninth compared to fifth) to be stably fit to the commingled dates, which more accurately resolves sedimentation rate changes. A ninth-order polynomial could not be stably fit to the core 2269 dates alone (Figure 3).

[27] The higher dating density in the upper part of core 2269, compared with core 2322, allowed the core 2322 age model to be significantly augmented with core 2269 dates (Figure 9a). Age differences between the core 2322 independent and commingled linearly interpolated age models are commonly around 100 years or less (Figure 9b). The largest age differences occur at around 8000 cal years B.P. (Figures 9a and 9b). The changing sedimentation rates in this interval were only constrained a single core 2322 date over a 5-m interval (Figure 3) with an unusually large uncertainty (1073 cm = 8000 ± 300 ^{14}C years B.P.; 8170, 8522, 8883 cal years B.P.) (Table 1). Three core 2269 dates augment the age model in this interval (Figure 9a). These refine the timing of the sedimentation rate changes and suggest that the median probable age of the core 2322 date; although it has large uncertainty, it provides a reliable age estimate (Tables 2 and 3).

[28] Sediment accumulation rates calculated using both linear interpolation between dates and polynomial fits for both cores are presented in Figures 8c and 9d. Both cores have substantially greater sediment accumulation rates in the older part of the records. For core 2322, the deglacial sedimentation rates of >4 m/kyr started decreasing after ca 9500 cal years B.P., arriving at Holocene background levels of $\sim$1 to 2 m/kyr after ca 8000 cal years B.P. (Figure 9d). For core 2269, the deglacial sedimentation rates of >3 m/kyr decline to Holocene background levels of $\sim$2 m/kyr by approximately 9500 cal years B.P. (Figure 8c). The different character and timing of sedimentation rate changes likely reflects the differing deglacial histories of these locations. Additional variations in sedimentation occur through the Holocene. Both cores show an increase in sedimentation rate over the last 1000 years, and core 2269 shows an increase centered at around 4000 cal years B.P. as well. The instantaneous sedimentation rates calculated from linear interpolation between dates (Figures 8c and 9d) indicate substantial variability that should be interpreted with caution when dates are so tightly spaced.

[29] The improved dating density of the commingled dates allows development of an age model for both cores with significantly less uncertainty than in either of the individual chronologies. Our preferred PSV/radiocarbon chronologies (referred to as 2269PSV-RC06* and 2322PSV-RC06*) (Figure 10) are based on linear interpo-

Figure 12. Cross-spectral analysis of weight percent calcium carbonate for cores MD99-2269 and MD99-2322 (Figure 11a) on their own independent and the PSV-RC06 chronologies. (a) Variance spectra of the core MD99-2269 carbonate record on its own (green) and on the PSV-RC06 (black) chronology. (b) Variance spectra of the core MD99-2322 carbonate record on its own (green) and on the PSV-RC06 (black) chronology. (c) Coherence spectra estimated from the independent (green) and PSV-RC06 chronologies (black). The 80% confidence line for nonzero coherence is indicated. (d) Phase calculations (only where coherence is nonzero at the 80% level) are shown for the carbonate records on their own independent (green) and PSV-RC06 chronologies (black).

lation between median probability ages for each date on the core 2269 depth scale (Figure 8a and Table 3). The PSV-RC06 chronology is transferred to core 2322 using the PSV correlation (Figure 9a). The $1-\sigma$ age uncertainties are shown as uncertainty envelopes in Figure 10. These are derived from the maximum age spread at each depth using either the linear interpolation or polynomial fits to the minimum and maximum $1-\sigma$ calibrated age ranges. This reflects the calibration and age model uncertainties at any particular depth. The PSV records on the PSV-RC06 chronology are also shown in Figure 10. The PSV-RC06 chronologies and PSV records are available through auxiliary material.[1]

5.2. Comparison of Paleoceanographic Proxies

[30] The PSV correlations are supported by the consistent interweaving of radiocarbon dates and by the correct alignment of the Saksunarvatn tephra (Figures 8 and 9). It is difficult to know objectively, however, if the relative correlation, the resulting commingled dates and the PSV-RC06 chronology are better. Another test of the PSV correlation and the PSV-RC06 chronology can be made using the $CaCO_3$ records. The total $CaCO_3$ content is interpreted as a proxy for productivity throughout the water column driven by coccolith and augmented by foraminiferal production [*Giraudeau et al.*, 2004]. This reflects both the contribution of Atlantic Water in the Irminger Current over the core sites, balanced by the outflow of Arctic and Polar surface waters. The similarity ($r = 0.89$) of the $CaCO_3$ records (Figure 2) of core 2269 (north Iceland continental margin) and 2322 (east Greenland continental margin) on their own independent timescales suggests that the two sites experienced similar Holocene paleoceanographic histories. This similarity is consistent with modern oceanography, as Irminger Intermediate Water similarly influences both sites. Therefore it seems reasonable to assume that the carbonate records could be similar over a range of timescales.

[31] When the $CaCO_3$ records are placed on the PSV-RC06 chronology (Figure 10), their correlation is $r = 0.895$ (Figure 11a, black line). This correlation is nearly identical to that obtained on their own independent chronologies ($r = 0.89$, green line), which reflects the dominance of the overall Holocene trend and the relatively minor adjustments to already strong age models. The Holocene trend is well described by a fifth-order polynomial fit to the $CaCO_3$ data (Figure 11a, green lines). On their independent chronologies, the correlation between the polynomial fit to $CaCO_3$ data is $r = 0.972$, while on the PSV-RC06 chronologies $r = 0.976$. Using the polynomial fit to subtract the long-term trend, we compare the detrended $CaCO_3$ data on independent chronology for each core, $r = 0.346$ (Figure 11b), and using the PSV-RC06 chronology, $r = 0.385$ (Figure 11c). Although not overwhelming, the improved correlation suggests that the two records are better aligned.

[32] The coherence spectrum provides another way to assess the correlation, by looking at how it varies as a function of frequency. We use the method described by *Schulz and Stattegger* [1997] designed for unevenly spaced paleoclimatic time series. The advantage of this method is the avoidance of data interpolation, which may underestimate high-frequency components. Cross-spectral analysis based on 11 degrees of freedom was calculated for the core 2269 and 2322 $CaCO_3$ data on their independent and PSV-RC06 chronologies (Figure 12). Coherence (Figure 12c) and phase spectra (Figure 12d) demonstrate that the carbonate records on the PSV-RC06 chronologies correlate, above the 80% confidence limit for nonzero coherence, over a range of frequencies extending through the centennial band. This is not the case when estimated on their own chronologies, which is well illustrated by the mean coherence, 0.41 for the PSV-RC06 chronologies, while only 0.18 when on their own independent timescales (Figure 12c). Placing the $CaCO_3$ records for core 2322 on the PSV-RC06 chronology results in a significant redistribution of variance from low to higher frequencies (Figure 12b) that correlates with the $CaCO_3$ record in core 2269. This supports the correlation and suggests that the intercalibration of radiocarbon and PSV provides a viable chronological strategy for studying high-accumulation-rate continental margin sediments. Phasing suggests some complexities and strongly supports higher-resolution data collection to better understand these dynamics.

6. Summary and Conclusions

[33] We have examined the intercalibration of paleomagnetic secular variation (PSV) records with a high density of calibrated radiocarbon dates. Two high-resolution *Marion Dufresne II* Calypso cores were studied that capture postglacial sediment sequences from the Denmark Strait region (Figure 1). Both cores are well dated, with 27 and 20 AMS ^{14}C dates for cores 2269 and 2322, respectively (Figure 3 and Table 1). Paleomagnetic measurements made on u channel samples document a strong, stable, single component magnetization that provides high-quality PSV records (Figure 4). Calibrated radiocarbon age models (Figure 3) document the temporal similarity of the paleomagnetic inclination and declination records for both cores (Figure 5). Detailed PSV comparisons reveal that relative correlations could still be improved. Starting in the depth domain, tie points, initially based on the radiocarbon dates, are either adjusted or added, to maximize inclination and declination correlation (Figures 6 and 7 and Table 2). Radiocarbon dates from both cores are then combined on a common core 2269 depth scale that results from the PSV correlation (Figure 8 and Table 3). Support for the correlation and the resulting chronologies come from consistent interweaving of dates (Figures 8a and 9a), correct alignment of the Saksunarvatn tephra and the statistically demonstrated improvement in correlation of paleoclimatic proxy data (e.g., weight percent $CaCO_3$) (Figures 11 and 12). No evidence for any systematic offsets that could be attributed to errors in correlation, differences in PSV lock-in depth or nonconsistent changes in radiocarbon reservoir age are observed.

[34] A new chronology (PSV-RC06) is developed by commingling dates from both cores on the common core

[1]Auxiliary materials are available at ftp://ftp.agu.org/apend/pa/2006pa001285.

2269 depth scale (Figure 10). PSV-RC06 can be transferred from core 2269 to core 2322 using the PSV correlation. The differences between the PSV-RC06 chronology (Figure 10) and the independent chronology for each core (Figure 3) are fairly small and no more than 170 and 330 years for cores 2269 and 2322, respectively (Figures 8b and 9b). The small changes reflect the quality of the independent chronology for each core, minimizing the impact of the PSV correlation. Conversely, the high density of radiocarbon dates on both cores provides an opportunity to test the level of synchronization provided by PSV correlation. Age offsets between the two chronologies (Figures 8 and 9) occur where dating density is low in one core or the other. The age models, rather than the dates (aside from the core catcher derived basal dates that are demonstrated to be too old), are the primary source of correlation and chronological error. PSV can substantially augment radiocarbon-based correlations and, in optimal settings, it can provide a level of synchronization on a par with what could be achieved by comparing two or more exceptionally well radiocarbon-dated records. PSV correlation, when used in conjunction with radiocarbon dates, can also improve regional chronologies by allowing dates from various stratigraphic sequences to be combined into a single, higher dating density, age-to-depth model.

[35] **Acknowledgments.** This research was supported by the National Science Foundation Office of Polar Programs grants ARC-0241291 to J.S.S. and ARC-0082347 to A.J. and Earth System History grant ATM-0317832 to A.J. We thank the captain and crew of the R/V *Marion Dufresne II* for collecting these sediments, Ken Verosub at UC Davis for use of his Paleomagnetism Laboratory, Nick Pisias for supplying spectral analysis code and advice, two anonymous reviewers and Andy Roberts for comments that improved the manuscript, and James Syvitski for welcoming J.S.S. to INSTAAR.

References

Aagaard, K., and L. K. Coachman (1968a), The East Greenland Current north of Denmark Strait: Part I, *Arctic*, *21*, 181–200.

Aagaard, K., and L. K. Coachman (1968b), The East Greenland Current north of Denmark Strait: Part II, *Arctic*, *21*, 167–290.

Andrews, J. T., G. Helgadottir, A. Geirsdottir, and A. E. Jennings (2001), Multicentury-scale records of carbonate (hydrographic?) variability on the northern Iceland margin over the last 5000 years, *Quat. Res.*, *56*, 199–206.

Andrews, J. T., A. Geirsdóttir, J. Hardardóttir, S. Principato, K. Grönvold, G. B. Kristjánsdóttir, G. Helgadóttir, J. Drexler, and A. Sveinbjörnsdóttir (2002), Distribution, sediment magnetism and geochemistry of the Saksunarvatn (10,180 ± 60 cal. yr B.P.) tephra in marine, lake, and terrestrial sediments, northwest Iceland, *J. Quat. Sci.*, *17*, 731–745.

Andrews, J. T., J. Hardadóttir, G. B. Kristjánsdóttir, K. Grönvold, and J. S. Stoner (2003), A very high resolution Holocene sediment record (5 yr/cm) from Húnaflóaáll, N Iceland margin: Century- to millennial-scale variability since the Vedde tephra, *Holocene*, *3*, 625–638.

Austin, W. E. N., E. Bard, J. B. Hunt, D. Kroon, and J. Peacock (1995), The ^{14}C age of the Icelandic Vedde Ash: Implications for Younger Dryas marine reservoir age corrections, *Radiocarbon*, *37*, 53–62.

Bard, E., M. Arnold, J. Mangerud, M. Paterne, L. Labeyrie, J. Duprat, M.-A. Melieres, E. Sonstegaard, and J.-C. Duplessy (1994), The North Atlantic atmosphere-sea surface ^{14}C gradient during the Younger Dryas climatic event, *Earth Planet. Sci. Lett.*, *126*, 275–287.

Birks, H. H., S. Gulliksen, H. Haflidason, J. Mangerud, and G. Possnert (1996), New radiocarbon dates from the Vedde Ash and Saksunarvatn Ash from western Norway, *Quat. Res.*, *45*, 119–127.

Björck, S., N. Koç, and G. Skog (2003), Consistently large marine reservoir ages in the Norwegian Sea during the last deglaciation, *Quat. Sci. Rev.*, *22*, 429–435.

Breckenridge, A., T. Johnson, S. Beske-Diehl, and J. S. Mothersill (2004), The timing of regional late glacial events and post-glacial sedimentation rates from Lake Superior, *Quat. Sci. Rev.*, *23*, 2355–2367.

Brooks, C. K. (1990), *Kangerdlugssuaq Studies: Processes at a Rifted Continental Margin*, edited by C. K. Brooks, Geol. Inst., Univ. of Copenhagen, Copenhagen.

Constable, C. G., and J. L. Johnson (2000), Global geomagnetic field models for the past 3000 years: Transient or permanent flux lobes?, *Philos. Trans. R. Soc. London, Ser. A*, *358*, 991–1008.

Dunhill, G., J. T. Andrews, and G. B. Kristjánsdóttir (Comps.) (2004), Radiocarbon Date List X: Baffin Bay, Baffin Island, Iceland, Labrador Sea, and the northern North Atlantic, *Occas. Pap. 56*, 77 pp., Inst. of Arct. and Alp. Res., Boulder, Colo.

Einarsson, T. (1973), Geology of Iceland, in *Arctic Geology*, edited M. G. Pitcher, *AAPG Mem.*, *19*, 171–175.

Ellison, C. R. W., M. R. Chapman, and I. R. Hall (2006), Surface and deep ocean interactions during the cold climate event 8200 years ago, *Science*, *312*, 1929–1932.

Giraudeau, J., A. E. Jennings, and J. T. Andrews (2004), Timing and mechanisms of surface and intermediate water circulation changes in the Nordic Seas over the last 10 000 cal. years: A view from the north Iceland shelf, *Quat. Sci. Rev.*, *23*, 2127–2139.

Grönvold, K., N. Oskarsson, S. J. Johnsen, H. B. Clausen, C. U. Hammer, G. Bond, and E. Bard (1995), Ash layers from Iceland in the Greenland GRIP ice core correlated with oceanic and land sediments, *Earth Planet. Sci. Lett.*, *135*, 149–155.

Guilderson, T. P., P. J. Reimer, and T. A. Brown (2005), The boon and bane of radiocarbon dating, *Science*, *307*, 362–364.

Hodell, D. A., M. Brenner, J. H. Curtis, and T. Guilderson (2001), Solar forcing of drought frequency in the Maya lowlands, *Science*, *292*, 1367–1370.

Hopkins, T. S. (1991), The GIN Sea—A synthesis of its physical oceanography and literature review 1972–1985, *Earth Sci. Rev.*, *30*, 175–318.

Hughen, K. A., et al. (2004), Marine04: Marine radiocarbon age calibration, 26–0 ka BP, *Radiocarbon*, *46*, 1059–1086.

Irurzun, M. A., C. S. G. Gogorza, M. A. E. Chaparro, J. M. Lirio, H. J. Nunez, F. Vilas, and A. M. Sinito (2006), Paleosecular variations recorded by Holocene-Pleistocene sediments from Lake El Trebol (Patagonia, Argentina), *Phys. Earth Planet. Inter.*, *154*, 1–17.

Jackson, A., A. R. T. Jonkers, and M. R. Walker (2000), Four centuries of geomagnetic secular variation from historical records, *Philos. Trans. R. Soc. London, Ser. A*, *358*, 957–990.

Jennings, A. E., K. Grönvold, R. Hilberman, M. Smith, and M. Hald (2002), High-resolution study of Icelandic tephras in the Kangerlussuq Trough, southeast Greenland, during the last deglaciation, *J. Quat. Sci.*, *7*, 747–757.

Jennings, A. E., M. Hald, M. Smith, and J. T. Andrews (2006), Freshwater forcing from the Greenland Ice Sheet during the Younger Dryas: Evidence from southeast Greenland shelf cores, *Quat. Sci. Rev.*, *25*, 282–298.

Johnsen, S. J., D. Dahl-Jensen, W. Dansgaard, and N. Gundestrup (1995), Greenland palaeotemperatures derived from GRIP bore hole temperature and ice isotope profiles, *Tellus, Ser. B*, *47*, 624–629.

Kirschvink, J. L. (1980), The least squares lines and plane analysis of paleomagnetic data, *Geophys. J. R. Astron. Soc.*, *62*, 699–718.

Korte, M., and C. G. Constable (2005), Continuous geomagnetic field models for the past 7 millennia: 2. CALS7K, *Geochem. Geophys. Geosyst.*, *6*, Q02H16, doi:10.1029/2004GC000801.

Korte, M., A. Genevey, C. G. Constable, U. Frank, and E. Schnepp (2005), Continuous geomagnetic field models for the past 7 millennia: 1. A new global data compilation, *Geochem. Geophys. Geosyst.*, *6*, Q02H15, doi:10.1029/2004GC000800.

Kotilainen, A. T., T. Saarinen, and B. Winterhalter (2000), High-resolution paleomagnetic dating of sediments deposited in the central Baltic Sea during the last 3000 years, *Mar. Geol.*, *166*, 51–64.

Kristjánsdóttir, G. B., J. S. Stoner, A. E. Jennings, J. T. Andrews, and K. Grönvold (2007), Geochemistry of Holocene cryptotephras from the North Iceland Shelf (MD99–2269): Intercalibration with radiocarbon and paleomagnetic chronostratigraphies, *Holocene*, *17*, 155–175.

Lund, S. P. (1996), A comparison of paleomagnetic secular variation records from North America, *J. Geophys. Res.*, *101*, 8007–8024.
Mangerud, J., H. Furnes, and J. Jóhansen (1986), A 9000-year old ash bed on the Faroe Islands, *Quat. Res.*, *26*, 262–265.
McMillan, D. G., C. G. Constable, and R. L. Parker (2002), Limitations on stratigraphic analyses due to incomplete age control and their relevance to sedimentary paleomagnetism, *Earth Planet. Sci. Lett.*, *201*, 509–523.
Meese, D., A. J. Gow, R. B. Alley, G. A. Zielinski, P. M. Grootes, M. Ram, K. C. Taylor, P. A. Mayewski, and J. F. Bolzan (1997), The Greenland Ice Sheet Project 2 depth-age scale: Methods and results, *J. Geophys. Res.*, *102*, 26,411–26,424.
Merrill, R. T., and P. L. McFadden (2003), The geomagnetic axial dipole field assumption, *Phys. Earth Planet. Inter.*, *139*, 171–185.
Mogensen, I. A. (2001), A study of rapid climate changes, Dansgaard-Oeschger events, Ph.D. thesis, Niels Bohr Inst., Univ. of Copenhagen, Copenhagen.
Nourgaliev, D. K., F. Heller, A. S. Borisov, I. Hajdas, G. Bonani, P. G. Iassonov, and H. Oberhansli (2003), Very high resolution paleosecular variation record for the last ~1200 years from the Aral Sea, *Geophys. Res. Lett.*, *30*(17), 1914, doi:10.1029/2003GL018145.
Ojala, A., and T. Saarinen (2002), Palaeosecular variation of the Earth's magnetic field during the last 10,000 years based on the annually laminated sediment of Lake Nautajärvi, central Finland, *Holocene*, *12*, 391–400.
Ojala, A. E. K., and M. Tiljander (2003), Testing the fidelity of sediment chronology: Comparison of varve and paleomagnetic results from Holocene lake sediments from central Finland, *Quat. Sci. Rev.*, *22*, 1787–1803.
Paillard, D., L. Labeyrie, and P. Yiou (1996), Macintosh program performs time-series analysis, *Eos Trans. AGU*, *77*, 379.
Reimer, P. J., et al. (2004), IntCal04 terrestrial radiocarbon age calibration, 26–0 ka B.P., *Radiocarbon*, *46*, 1029–1058.
Saarinen, T. (1999), Paleomagnetic dating of late Holocene sediments in Fennoscandia, *Quat. Sci. Rev.*, *18*, 889–897.
Schulz, M., and K. Stattegger (1997), Spectrum: Spectral analysis of unevenly spaced paleoclimatic time series, *Comput. Geosci.*, *23*, 929–945.
Skinner, L. C., and I. N. McCave (2003), Analysis and modelling of gravity- and piston coring based on soil mechanics, *Mar. Geol.*, *199*, 181–204.
Snowball, I., and P. Sandgren (2002), Geomagnetic field variations in northern Sweden during the Holocene from varved lake sediments and their implications for cosmogenic nuclide production rates, *Holocene*, *12*, 517–530.
Snowball, I., and P. Sandgren (2004), Geomagnetic field intensity changes in Sweden between 9000 and 450 cal B.P.: Extending the record of archaeomagnetic jerks by means of lake sediments and the pseudo-Thellier technique, *Earth Planet Sci. Lett.*, *227*, 361–376.
Sowers, T., M. Bender, L. Labeyrie, D. Martinson, J. Jouzel, D. Raynaud, J. J. Pichon, and Y. S. Korotkevich (1993), A 135,000 year Vostok-SPECMAP common temporal framework, *Paleoceanography*, *8*, 737–766.
Stefansson, U. (1962), North Icelandic waters, *Rit Fiskideildar*, *3*, 269 pp.
Stockhausen, H. (1998), Geomagnetic paleosecular variation (0–13 000 yr B.P.) as recorded in sediments from three maar lakes from the West Eifel (Germany), *Geophys. J. Int.*, *135*, 898–910.
St-Onge, G., J. S. Stoner, and C. Hillaire-Marcel (2003), Holocene paleomagnetic records from the St. Lawrence Estuary, eastern Canada: Centennial to millennial-scale geomagnetic modulation of cosmogenic isotopes, *Earth Planet. Sci. Lett.*, *209*, 113–130.
St-Onge, G., D. J. W. Piper, T. Mulder, C. Hillaire-Marcel, and J. S. Stoner (2004), Earthquake and flood-induced turbidites in the Saguenay Fjord (Québec): A Holocene paleoseismicity record, *Quat. Sci. Rev.*, *23*, 283–294.
Stuiver, M., and P. J. Reimer (1993), Extended ^{14}C database and revised CALIB radiocarbon calibration program, *Radiocarbon*, *35*, 215–230.
Stuiver, M., P. J. Reimer, E. Bard, J. W. Beck, K. A. Hughen, B. Kromer, F. G. McCormack, J. van des Plicht, and M. Spurk (1998), INTCAL98 radiocarbon age calibration 24,000–0 cal. BP, *Radiocarbon*, *40*, 1041–1083.
Telford, R. J., E. Heegaard, and H. J. B. Birks (2004), All age-depth models are wrong: But how badly?, *Quat. Sci. Rev.*, *23*, 1–5.
Thompson, R. (1973), Palaeolimnology and paleomagnetism, *Nature*, *242*, 182–184.
Thompson, R. (1984), A global review of paleomagnetic results from wet lake sediments, in *Lake sediments and Environmental History*, edited by E. Y. Haworth and J. W. G. Lund, pp. 145–165, Univ. of Minn. Press, Minneapolis.
Thouveny, N., E. Moreno, D. Delanghe, L. Candon, Y. Lancelot, and N. J. Shackleton (2000), Rock magnetic detection of distal ice-rafted debris: Clue for the identification of Heinrich layers on the Portuguese margin, *Earth Planet. Sci. Lett.*, *180*, 61–75.
Turner, G. M., and R. Thompson (1981), Lake sediment record of the geomagnetic secular variation in Britain during Holocene times, *Geophys. J. R. Astron. Soc.*, *65*, 703–725.
Turon, J. L., and C. Hillaire-Marcel (1999), Les rapports de campagnes à la mer IMAGES V à bord du *Marion Dufresne* 2e Leg du 30 juin au 24 juillet, *Geol. Surv. Can. Open File 3782*, Nat. Reour. Can., Ottawa, Ont. (Available at http://www.unites.uqam.ca/geotop/rapport/imagesV_leg2/eng/cruise_report.shtml)
Vigliotti, L. (2006), Secular variation record of the Earth's magnetic field in Italy during the Holocene: Constraints for the construction of a master curve, *Geophys. J. Int.*, *165*, 414–429.
Wang, Y., H. Cheng, R. L. Edwards, Y. He, X. Kong, Z. An, J. Wu, M. J. Kelly, C. A. Dykoski, and X. Li (2005), The Holocene Asian monsoon: Links to solar changes and North Atlantic climate, *Science*, *308*, 854–857.
Weeks, R. J., C. Laj, L. Endignoux, M. D. Fuller, A. P. Roberts, R. Manganne, E. Blanchard, and W. Goree (1993), Improvements in long core measurement techniques: Applications in palaeomagnetism and palaeoceanography, *Geophys. J. Int.*, *114*, 651–662.

J. T. Andrews, G. Dunhill, A. Jennings, and G. B. Kristjánsdóttir, Institute of Arctic and Alpine Research, Boulder, CO 80309-0450, USA.

J. Hardardóttir, National Energy Authority, Grensasvegur 9, Reykjavik, 108 Iceland.

J. S. Stoner, College of Oceanic and Atmospheric Sciences, Oregon State University, 104 COAS Administration Building, Corvallis, OR 97331-5503, USA. (jstoner@coas.oregonstate.edu)